Gondwana Research 36 (2016) 439–458

Contents lists available at ScienceDirect

Gondwana Research

journal homepage: www.elsevier.com/locate/gr

Granites of the intracontinental termination of a magmatic arc: an example from the Ediacaran Araçuaí orogen, southeastern Brazil

Leonardo Gonçalves [a,*], Fernando F. Alkmim [a], Antônio C. Pedrosa-Soares [b], Ivo A. Dussin [b], Claudio de M. Valeriano [c], Cristiano Lana [a], Mahyra Tedeschi [b]

[a] Departamento de Geologia, Escola de Minas, Universidade Federal de Ouro, Morro do Cruzeiro, 35400-000 Ouro Preto, MG, Brazil
[b] Universidade Federal de Minas Gerais, Programa de Pós-Graduação em Geologia, CPMTC-IGC-UFMG, Av. Antônio Carlos 6627, Pampulha, 31270-901 Belo Horizonte, MG, Brazil
[c] TEKTOS, Geotectonics Study Group, Universidade do Estado do Rio de Janeiro, Rua São Francisco Xavier 524/4006-A, 20559-900 Rio de Janeiro, RJ, Brazil

ARTICLE INFO

Article history:
Received 28 January 2015
Received in revised form 7 July 2015
Accepted 29 July 2015
Available online 29 August 2015

Handling Editor: A.S. Collins

Keywords:
Granites
Magmatic arc termination
Ediacaran
Rio Doce arc
Araçuaí orogen

ABSTRACT

The Araçuaí orogen of southeastern Brazil together with the West Congo belt of central West Africa form the Araçuaí–West Congo orogen generated during closure of a terminal segment of the Neoproterozoic Adamastor Ocean. Corresponding to an embayment in the São Francisco–Congo Craton, this portion of the Adamastor was only partially floored by oceanic crust. The convergence of its margins led to the development of the Rio Doce magmatic arc between 630 Ma and 580 Ma. The Rio Doce magmatic arc terminates in the northern portion of the Araçuaí orogen. Granitic plutons exposed in the northern extremity of the arc provide a rare opportunity to study magmatism at arc terminations, and to understand the interplay between calc-alkaline magma production and crustal recycling. The plutons forming the terminus of the arc consist of granodiorites, tonalites and monzogranites similar to a magnesian, slightly peraluminous, calcic- (68%) to calc-alkaline (24%), with minor alkali-calcic (8%) facies, medium- to high-K magmatic series. Although marked by negative Nb–Ta, Sr and Ti anomalies, typically associated with subduction-related magmas, the combined Sr, Nd and Hf isotopic data characterize a crustal signature related to anatexis of metamorphosed igneous and sedimentary rocks, rather than fractional crystallization of mantle-derived magmas. Zircon U–Pb ages characterizes two groups of granitoids. The older group, crystallized between 630 and 590 Ma, experienced a migmatization event at ca. 585 Ma. The younger granitoids, emplaced between 570 and 590 Ma, do not show any evidence for migmatization. Most of the investigated samples show good correlation with the experimental compositional field of amphibolite dehydration-melting, with some samples plotting into the field of greywacke dehydration-melting. The studied rocks are not typical I-type or S-type granites, being particularly similar to transitional I/S-type granitoids described in the Ordovician Famatinian arc (NW Argentina). We suggest a hybrid model involving dehydration-melting of meta-igneous (amphibolites) and metasedimentary (greywackes) rocks for magma production in the northern termination of the Rio Doce arc. The real contribution of each end-member is, however, a challenging work still to be done.

1. Introduction

Major and trace element data, together with Lu–Hf in zircon, whole-rock Sm–Nd and Rb–Sr isotopes provide sensitive discriminators of tectonic and/or magmatic processes operating above subduction zones and within collisional orogens (Rudnick, 1995; Kemp and Hawkesworth, 2003; Kemp et al., 2006; Liu et al., 2013; Niu et al., 2013). These chemistry and isotope datasets can also be used to discriminate between a range of geological processes involved in the pre-collisional to collisional stages of an orogenic belt evolution, such as crustal reworking, crust–mantle interactions, and production of juvenile magmas from the mantle.

The Araçuaí orogen of southeastern Brazil and the West Congo belt of southwestern Africa once lie in the central portion of West Gondwana (Alkmim et al., 2001). Together, they form the Araçuaí–West Congo orogen (AWCO), generated during closure of a terminal branch of the Neoproterozoic Adamastor Ocean (Pedrosa-Soares et al., 1992, 2001; Brito Neves et al., 1999; Cordani et al., 2003; Alkmim et al., 2006). Emplacement of ophiolite slivers, development of intra-oceanic and continental-margin magmatic arcs, and collision of the plates represented by the São Francisco–Congo, Paranapanema, Rio de la Plata and Kalahari cratons record the Adamastor Ocean closure from the Cryogenian to Ediacaran periods (e.g., Pedrosa-Soares et al., 1998, 2011; Campos-Neto, 2000; Alkmim et al., 2001, 2006; Basei et al.,

* Corresponding author. Tel.: +55 31 87101840.
E-mail addresses: leonardogeologo@hotmail.com, leonardo@degeo.ufop.br (L. Gonçalves), ffalkmim@gmail.com (F.F. Alkmim), pedrosa@pq.cnpq.br (A.C. Pedrosa-Soares), ivodusin@yahoo.com.br (I.A. Dussin), cmval@uerj.br (C.M. Valeriano), cristianodeclana@gmail.com (C. Lana), mahyratedeschi@gmail.com (M. Tedeschi).

http://dx.doi.org/10.1016/j.gr.2015.07.015
1342-937X/

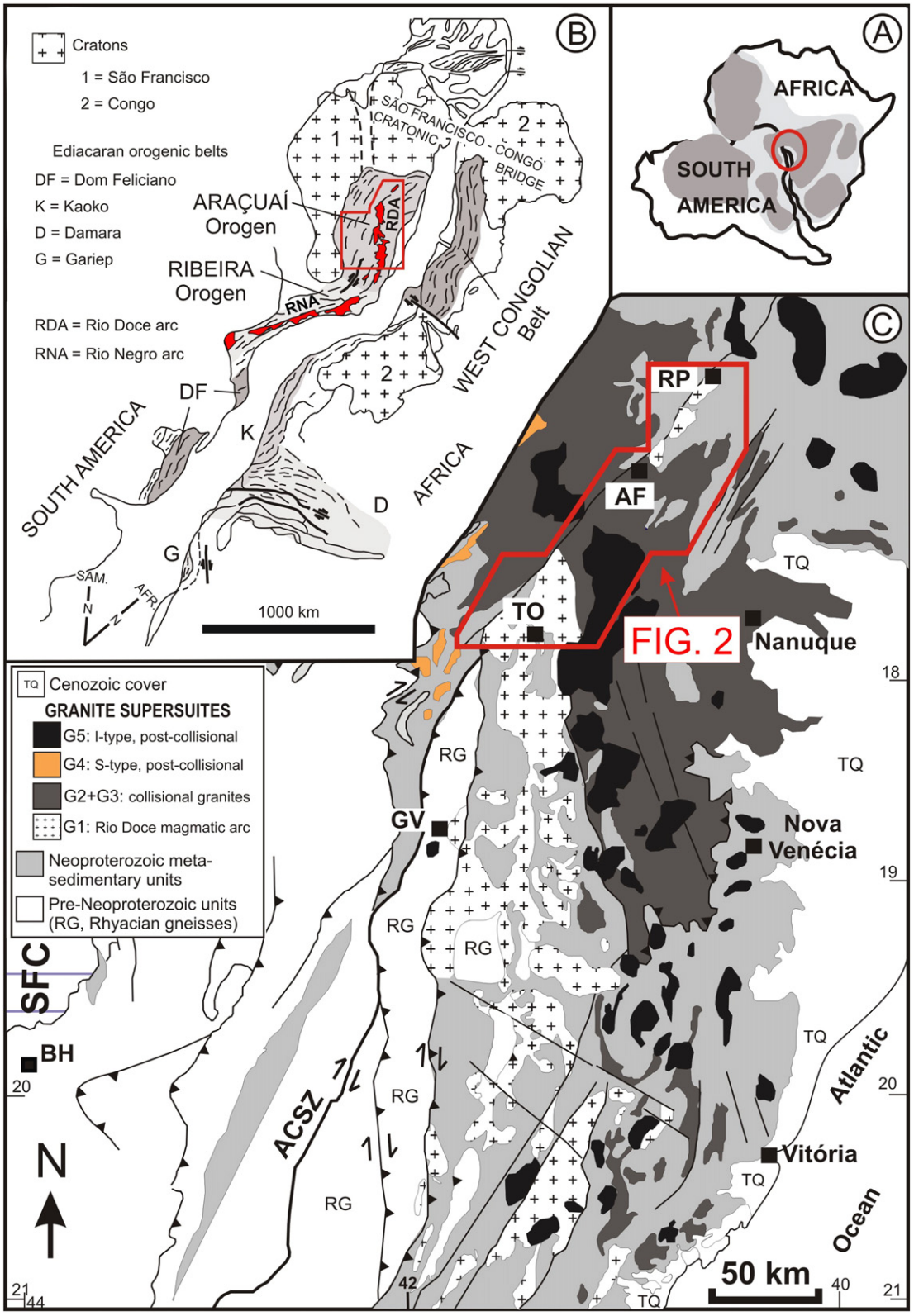

Fig. 1. A) The Araçuaí–West Congo orogen and related cratons in the context of West Gondwana (after Alkmim et al., 2006; Noce et al., 2007). Dark gray = cratons; light gray = orogenic belts. B) Relative positions of the Neoproterozoic orogenic belts (in gray) presently exposed along the South American and African margins of the Atlantic (modified from Porada, 1989). Red polygon and regions indicate, respectively, the approximate location of Fig. 1C and plutons forming the Rio Doce and Rio Negro arcs. C) Simplified geological map of the Araçuaí orogen, with a box indicating the studied region (modified from Pedrosa-Soares et al., 2008). ACSZ = Abre Campo Shear Zone; SFC = São Francisco Craton. Cities: BH = Belo Horizonte; GV = Governador Valadares; TO = Teófilo Otoni; AF = Águas Formosas; RP = Rio do Prado.

2010; Tupinambá et al., 2012; Heilbron et al., 2013). Representing the northern segment of the Adamastoran orogenic system (e.g., Goscombe and Gray, 2008), the AWCO exhibits a very peculiar configuration (Fig. 1), as it ended against a continental bridge linking the basement counterparts located in Bahia state (eastern Brazil) and Gabon (West Africa), the São Francisco–Congo cratonic bridge (Torquato and Cordani, 1981; Porada, 1989). In spite of this unique tectonic setting, the AWCO exhibits Late Cryogenian to Ediacaran ophiolite slivers and the Ediacaran Rio Doce magmatic arc, suggesting that its precursor was a gulf-like inland-sea embayment partially floored by oceanic crust (e.g., Pedrosa-Soares et al., 1998, 2011; Nalini et al., 2000; Alkmim et al., 2006; Queiroga et al., 2007).

The exhumed crystalline core of the Araçuaí orogen exposes a whole series of calc-alkaline plutons dated between 630 Ma and 580 Ma and grouped in the G1 Supersuite (Figs. 1 and 2), which represents the plutonic part of the Rio Doce magmatic arc (Figueiredo and Campos Neto, 1993; Nalini et al., 2000; Pedrosa-Soares and Wiedemann-Leonardos, 2000; Pedrosa-Soares et al., 2011; Gonçalves et al., 2014).

Magmatic arcs developed along active margins rarely died out in intracontinental domains. Because of the peculiar tectonic setting of the AWCO, the G1 Supersuite plutons exposed in the northern Araçuaí orogen apparently mark the termination of the Rio Doce arc in a continental setting (Figs. 1 and 2). What is the chemical signature of granites formed in a magmatic arc dying out in an intracontinental domain? Are they chemically similar to granites formed in arcs developed on active plate margins or more akin to collisional granites? What is the extent of crustal–mantle interaction and crustal recycling in such a highly ensialic setting? The G1 plutons of the northern Araçuaí orogen constitute a unique natural laboratory for providing answers to these questions and investigating features and process not yet well documented in the literature. In this paper, we present results of a detailed field, petrological, geochemical and geochronological study performed on G1 Supersuite plutons exposed in the northern end of the Rio Doce arc. In order to discuss the nature of the granitic rocks generated in this particular setting, we compare our results with geochemical datasets from other segments of the Rio Doce arc and arc-related granites worldwide.

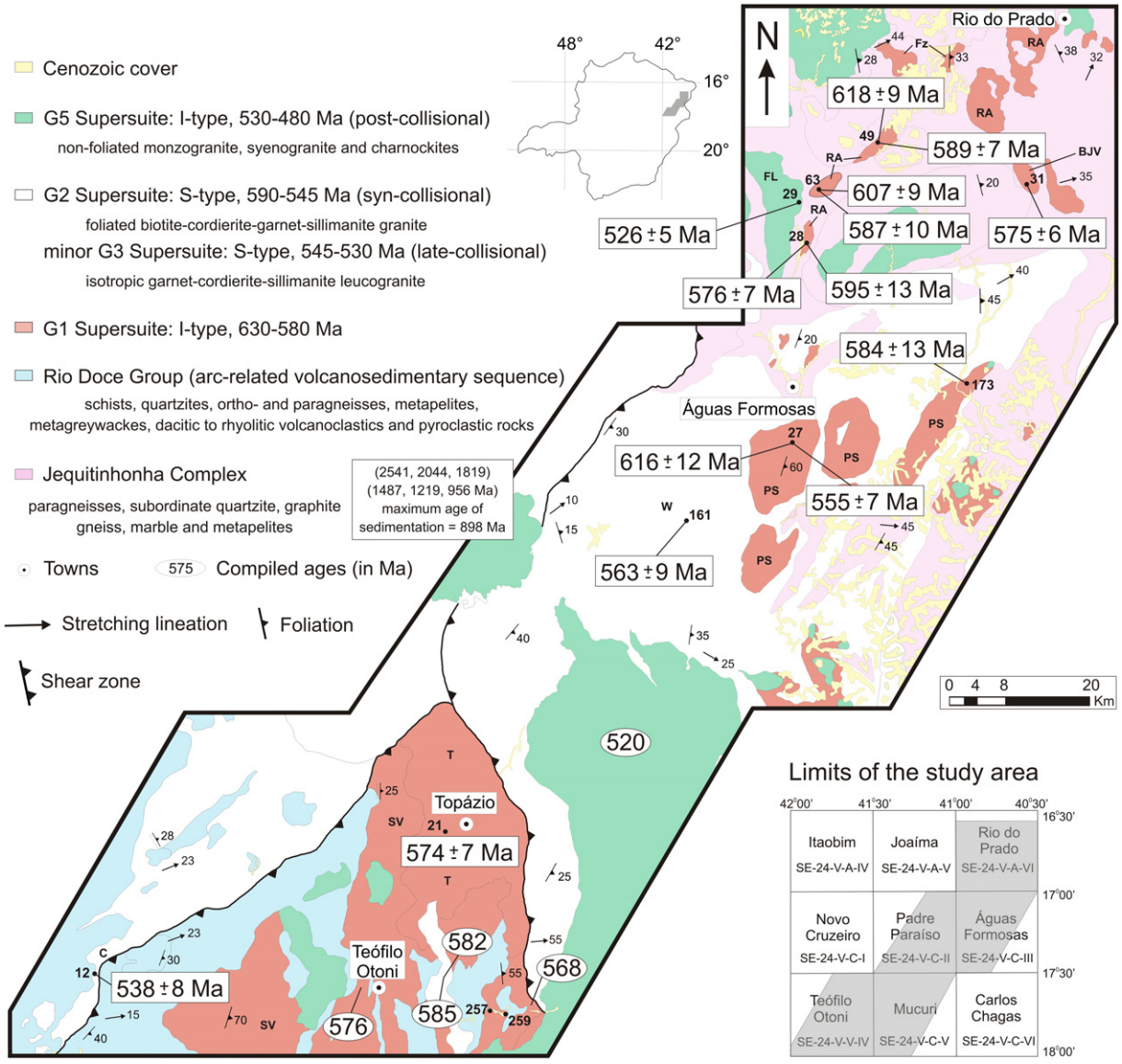

Fig. 2. Simplified geological map of the study area showing the sample sites for petrographic, geochemical, isotopic and geochronological analyses. The studied and dated plutons are: RA = Rancho Alegre (samples LG28, LG49 and LG63), Fz = Felizburgo, BJV = Bom Jesus da Vitória (sample LG31), PS = Pedra do Sino (samples LG27 and LG173), SV = São Vítor, T = Topázio (sample LG21), W = Wolff (sample LG161), C = Caraí (sample LG12) and Fazenda Liberdade (sample LG29). For simplicity the samples are shown on the map just with numbers. See text for further details.

2. Geological setting

The area we selected for study, encompassing a segment of ca. 10,000 km^2 of the crystalline core of the Araçuaí orogen, is located between 16°30′ and 18°00′ S Lat., and 40°30′ and 42°00′ W Long., i.e., between the towns of Teófilo Otoni and Rio do Prado in northeastern Minas Gerais State, Brazil (Figs. 1 and 2). We chose this region because it is entirely covered by geologic maps (Fontes, 2000; Moreira, 2000; Paes, 2000; Sampaio, 2000; Gomes, 2008; Paes et al., 2010) and contains good exposures of the northernmost plutons of the G1 Supersuite (Fig. 2).

The evolution of the Araçuaí orogen between the Early Ediacaran up to the Cambrian–Ordovician boundary produced an enormous volume of granitoids (including their Opx-bearing equivalents) and subordinate mafic rocks. Using field relationships, structural features, chemical and geochronological data, these igneous rocks were grouped into five assemblages, the G1, G2, G3, G4 and G5 supersuites (Pedrosa-Soares et al., 2011).

The granitic rocks forming the G1 Supersuite in the study area intrude with diffuse and sharp contacts the metasedimentary rocks of the Jequitinhonha Complex and the meta-volcanosedimentary Rio Doce Group, and are in turn cut by granites of the G2, G3 and G5 supersuites (Fig. 2).

Representing the oldest rock assemblage in the study area, the Jequitinhonha Complex (Fig. 2) consists of garnet–biotite gneisses, kinzigites, quartzites, graphite-rich gneisses, marbles, and metamafic rocks (Almeida and Litwinski, 1984; Paes et al., 2010; Gonçalves-Dias et al., 2011). U–Pb determinations on detrital zircon grains from a quartzite intercalated with the paragneisses have yielded a maximum depositional age of 898 ± 8 Ma for protoliths of the complex (Gonçalves-Dias et al., 2011), which are interpreted as high grade equivalents of the Araçuaí orogen type unit, the Tonian–Cryogenian Macaúbas Group (Pedrosa-Soares et al., 2008; Gonçalves-Dias et al., 2011, and references therein).

The Rio Doce Group crops out in the southwestern portion of the study area (Fig. 2), and comprises pelitic schists, quartzites, paragneisses, and metagreywackes. The group also contains dacitic and rhyolitic rocks dated around 585 Ma (Vieira, 2007; Gonçalves et al., 2010, 2014). The maximum depositional age of the group, estimated at 594 ± 3 Ma, was constrained by the ages of detrital zircons extracted from schists and metagreywackes (Vieira, 2007). Field observations and petrographic studies led Vieira (2007), Pedrosa-Soares et al. (2011), and Gonçalves et al. (2010, 2014) to interpret the volcanic rocks of this unit as equivalent to the G1 rocks and the group as a whole as a Rio Doce arc cover succession.

In the study area, the G1 Supersuite includes small plutons (up to 5 km^2) and stocks (up to 80 km^2). The main bodies, known as Rancho Alegre, Felizburgo, Pedra do Sino, Bom Jesus da Vitória, São Vítor and Topázio (Fig. 2), consist of tonalites (including Opx-bearing terms), granodiorites, and minor monzogranites. They are essentially peraluminous rocks (the ASI average is 1.07), involving calcic (68%), calc-alkaline (24%) and alkali-calcic (8%) facies, occasionally containing titanite or garnet, but commonly without hornblende. These rocks are isotropic to foliated, with local migmatitic features, and host both meta-igneous and metasedimentary enclaves, being the latter by far the more frequent (e.g., Paes et al., 2010 and references therein).

In the remaining portions of the Araçuaí orogen, the G1 Supersuite consists of medium- to high-K, calc-alkaline, tonalitic to granitic bodies (including their Opx-bearing equivalents), and subordinate mafic to intermediate plutons containing gabbroic to enderbitic facies (Novo et al., 2010; Tedeschi, 2013; Gonçalves et al., 2014). Typical for the majority of the G1 rocks is a large population of mafic enclaves (Nalini et al., 2000; Gonçalves et al., 2010, 2014; Pedrosa-Soares et al., 2011). All these characteristics, together with the pre-collisional nature of the G1 Supersuite, led most authors to interpret this rock assemblage as representative of a continental magmatic arc (e.g., Nalini et al., 2000, 2005; Pedrosa-Soares and Wiedemann-Leonardos, 2000; Pedrosa-Soares et al., 2001, 2008, 2011; Martins et al., 2004; Gonçalves et al., 2010, 2014; Novo et al., 2010; Tedeschi, 2013), named Rio Doce arc by Figueiredo and Campos Neto (1993). The development of the Rio Doce arc, constrained by zircon U–Pb ages between 630 and 580 Ma, is viewed as a consequence of the consumption of the oceanic segment of the Adamastor terminal branch, which took place before the collisional event that led to the full development of the AWCO (Pedrosa-Soares et al., 1998, 2001, 2008; Alkmim et al., 2006; Gonçalves et al., 2014).

The G2 Supersuite occurs in the form of isolated plutons or batholiths mainly in the central and southern portions of the study area (Fig. 2), where foliated biotite–cordierite–garnet–sillimanite granites predominate (Gradim et al., 2014). Made up essentially of S-type granites, the G2 Supersuite show U–Pb ages between 590 Ma and 545 Ma (e.g., Nalini et al., 2000; Pedrosa-Soares and Wiedemann-Leonardos, 2000; Pedrosa-Soares et al., 2011; Gradim et al., 2014). This interval corresponds to the main phase of deformation and metamorphism recorded in the Araçuaí orogen (Silva et al., 2002, 2011; Alkmim et al., 2006; Pedrosa-Soares et al., 2011; Gonçalves et al., 2014; Gradim et al., 2014).

Commonly associated with the G2 rocks, the G3 Supersuite is made up of isotropic garnet–cordierite–sillimanite leucogranites. Mostly composed of S-type granites, the G3 rocks are not individualized in the study area, due to limitations on the scale of mapping. Its magmatic crystallization is constrained by zircon ages between 545 Ma and 530 Ma, representing the late-collisional stage of the Araçuaí orogen (Pedrosa-Soares et al., 2011; Gradim et al., 2014).

The G4 Supersuite occurs as zoned plutons or batholiths in the region to the south of the study area (Fig. 1) and consists of non-foliated biotite granite, two-mica and muscovite–garnet leucogranites. Commonly, G4 plutons show igneous flow structures and are peraluminous. Zircon U–Pb data constrain the magmatic crystallization age of the S-type G4 granitoids between 530 Ma and 500 Ma (e.g., Pedrosa-Soares et al., 2011 and references therein). According to Alkmim et al. (2006) and Pedrosa-Soares et al. (2011), together with the G5 Supersuite, the G4 granites represent the product of a magmatic event related to the orogenic collapse phase of the Araçuaí orogen.

The G5 Supersuite occurs as small or large plutons widespread in the study area (Fig. 2), and consists of non-foliated monzogranite, syenogranite, and charnockites. Locally, these granitoids are foliated close to their contact with the older units. U–Pb data on zircon grains from the study area combined with ages from different parts of the orogen constrain the crystallization ages of the I-type G5 granitoids between 530 Ma and 480 Ma (e.g., De Campos et al., 2004; Pedrosa-Soares et al., 2011).

3. Analytical methods

Representative samples of the G1 Supersuite granitoids were chosen for lithochemical (8 samples), geochronological (U–Pb — 10 samples, Lu–Hf — 4 samples) and isotopic (Sm–Nd, Rb–Sr — 6 samples) analyses. Additionally, two samples of the G2 rocks and one sample of the G5 Supersuite were dated (U–Pb zircon analyses). Care was taken to select fresh and homogenous parts of the samples, avoiding weathered, metamorphosed, or late veins. All the samples were crushed and milled at the Departamento de Geologia of the Universidade Federal de Ouro Preto, Brazil. Major, trace and rare earth element (REE) concentrations were determined at the ACME Analytical Laboratory LTDA, Vancouver, Canada. Major oxides were analyzed via inductively coupled plasma atomic emission spectroscopy (ICP-AES) after fusion with lithium metaborate–tetraborate and digestion with diluted nitric acid. Trace and REE concentrations were analyzed via inductively coupled plasma mass spectrometry (ICP-MS) adopting the same procedure previously mentioned as for major oxides. Detection limits are 0.01% for oxides and 0.1–0.01 ppm for trace, and rare earth elements. The loss on ignition (LOI) was determined by the weighting difference after ignition at 1000 °C. The geochemical dataset of samples from the literature as

Table 1
Summary of the key main features of the Jequitinhonha paragneisses and G1 granitic rocks exposed in the study area.

Unit	Rock type	Mineralogy		Geochemistry	Field observations	References
		Main minerals	Accessory minerals			
Jequitinhonha Complex	Paragneiss	Quartz, feldspar, biotite, cordierite, garnet (almandine)	Sillimanite, graphite, opaques	Peraluminous gneisses, with pelitic greywackes as probable protolith	Banded, migmatized	Gonçalves-Dias et al. (2011)
	Biotite paragneiss, Al-rich gneiss	Quartz, plagioclase, K-feldspar, biotite, cordierite, garnet	Sillimanite, zircon, apatite, graphite, muscovite, opaques		Foliated, banded, migmatized	Paes et al. (2010)
Rancho Alegre plutons	Tonalite, minor granodiorite and monzogranite	Plagioclase, quartz, K-feldspar, biotite	Apatite, zircon, monazite, garnet, opaques	Slightly peraluminous, mostly medium-K calc-alkaline	Isotropic to foliated, locally migmatized	Paes et al. (2010)
Felizburgo plutons	Granodiorite, minor tonalite and monzogranite	Plagioclase, quartz, orthoclase, microcline, biotite	Apatite, zircon, opaques (e.g., magnetite), monazite, titanite, allanite	Slightly peraluminous, mostly medium- to high-K calc-alkaline	Foliated, migmatized	
Pedra do Sino plutons	Monzogranite, granodiorite and tonalite	Quartz, microcline, orthoclase, plagioclase, biotite	Garnet, allanite, epidote, apatite, zircon, opaques, titanite, monazite, muscovite, sillimanite	Not available	Isotropic to strongly foliated	Carvalho and Pereira (2000)
São Vitor plutons	Granodiorite and tonalite, minor monzogranite and syenogranite	Plagioclase, microcline, orthoclase, quartz, biotite	Garnet, allanite, titanite, apatite, zircon, monazite, rutile, opaques	Metaluminous to slightly peraluminous	Isotropic to foliated, and banded	
Topázio plutons	Granodiorite, minor monzogranite					
G1 Supersuite (Rancho Alegre, Felizburgo, Pedra do Sino, São Vitor, Topázio, Bom Jesus da Vitória plutons)	Granodiorite and tonalite, minor monzogranite	Plagioclase, quartz, orthoclase, microcline, biotite, hornblende	Zircon, apatite, monazite, garnet, titanite, allanite, epidote, rutile, muscovite, hematite, ilmenite, magnetite, pyrrhotite, chalcopyrite	Magnesian, mostly slightly peraluminous, and calcic to calc-alkalic, medium- to high-K acid-silicic plutonic rocks	Isotropic to foliated, locally migmatized	This study

well as data from this study are presented as Supplementary data — item 1.

U–Pb zircon laser ablation multicollector inductively coupled plasma mass spectrometry (LA–MC–ICP–MS, Neptune Thermo Scientific) analyses were carried out at the Geochronology Laboratory of the Universidade de São Paulo, Brazil. Samples were prepared for analysis in laboratories of Universidade Federal de Ouro Preto and Universidade de São Paulo, Brazil. Zircon grains were separated using conventional methods (crushing, grinding, gravimetric and magnetic-Frantz isodynamic separator), and handpicked under binocular microscope. Only zircon crystals from the least magnetic fractions were selected for geochronological analysis. Selected zircon grains were mounted in an epoxy disk and polished to expose the interiors. The morphology and internal structure of zircons were characterized by optical microscopy and cathodoluminescence (CL) imaging. The mount disks were then cleaned and the U–Pb isotopic compositions of zircon were analyzed. A spot size of 25 μm was applied to all analyses. Zircon GJ-1 (Jackson et al., 2004) was used as an external standard and was analyzed twice every 6 analyses. Analytical spots were conducted avoiding grain areas with inclusions, fractures and metamictic structures. Data reduction used the Excel sheet developed by Chemale et al. (2012). For all samples the data of each spot was evaluated taking into account the common Pb contents, errors of isotopic ratios, percentages of discordance and Th/U ratios. Selected spots used for age calculations were those with discordance lower than 10%. Concordia diagrams were obtained with the software Isoplot/Ex (Ludwig, 2003). U–Pb analytical data and concordia diagrams are shown as Supplementary data — item 2 and in Fig. 10.

The Sm–Nd (ID-TIMS) and Sr (natural) isotope analyses were performed in the Geochronology and Radiogenic Isotope Laboratory (LAGIR) at UERJ, the Rio de Janeiro State University. The analyzed samples were 4 granodiorites, 1 tonalite and 1 enderbite belonging to the G1 Supersuite, and the results are shown as Supplementary Data — item 3 and in Fig. 11. Clean rooms were used with positive air pressure and double-HEPA air filtering. Each rock powder sample weighting up to 50 mg was mixed with an isotope tracer solution of ^{149}Sm and ^{150}Nd in Savillex™ PTFE beakers. Chemical digestion of samples (plus tracer) by a mixture of HF (6 mL) and HNO_3 6 N (0.5 mL) on a hot plate, lasted 2 periods of 5 days. A primary phase of chromatographic extraction of Sr and REE in HCl used an ion exchange column filled with the BIORAD AG50W-X8 resin (100–200 mesh). The extraction of Sm and Nd from the REE solution was done with the Eichrom LN-spec resin (150 mesh) in a smaller column. The samples were then loaded separately onto previously degassed Re filament in double assembly, using H_3PO_4 (1 N) as the ionization activator. The Sm, Nd and Sr isotope ratios were measured with the multi-collector TRITON thermal ionization mass spectrometer (TIMS), in cup configurations of up to 8 Faraday collectors in static mode. The measured isotope ratios were normalized to the respective constant isotope ratios of $^{147}Sm/^{152}Sm = 0.56083$, $^{146}Nd/^{144}Nd = 0.7219$ and $^{86}Sr/^{88}Sr = 0.1194$. Corrections were applied for instrumental bias, tracer content and blanks below 200 pg Nd, and 70 pg Sm. Repeated analyses (n = 140) of the NBS-987 (NIST) and (n = 214) of the Jnd1 (Tanaka et al., 2000) standard reference materials yielded mean ratios $^{87}Sr/^{86}Sr = 0.710239 \pm 0.000007$ and $^{143}Nd/^{144}Nd = 0.512100 \pm 0.000006$ (2σ absolute standard errors), respectively. The Sm–Nd T_{DM} model ages and the $\varepsilon_{Nd(i)}$ values were calculated using DePaolo's (1981) parameters.

Lu–Hf analyses in zircon were obtained via laser ablation multicollector inductively coupled plasma mass spectrometry (LA–MC–ICP–MS, Photonmachines 193/Neptune Thermo Scientific) at the Isotope Geochemistry Laboratory of the Departamento de Geologia of the Universidade Federal de Ouro Preto, Brazil. The analyzed samples were 3 granodiorites and 1 enderbite, and the results are presented as Supplementary data — item 4, and in Fig. 12. Data were collected in static mode during 60 s of ablation with a spot size of 50 μm. Nitrogen (~0.080 L/min) was introduced into the Ar sample carrier gas. Typical signal intensity was ca. 12 V for ^{180}Hf. The isotopes ^{172}Yb, ^{173}Yb and

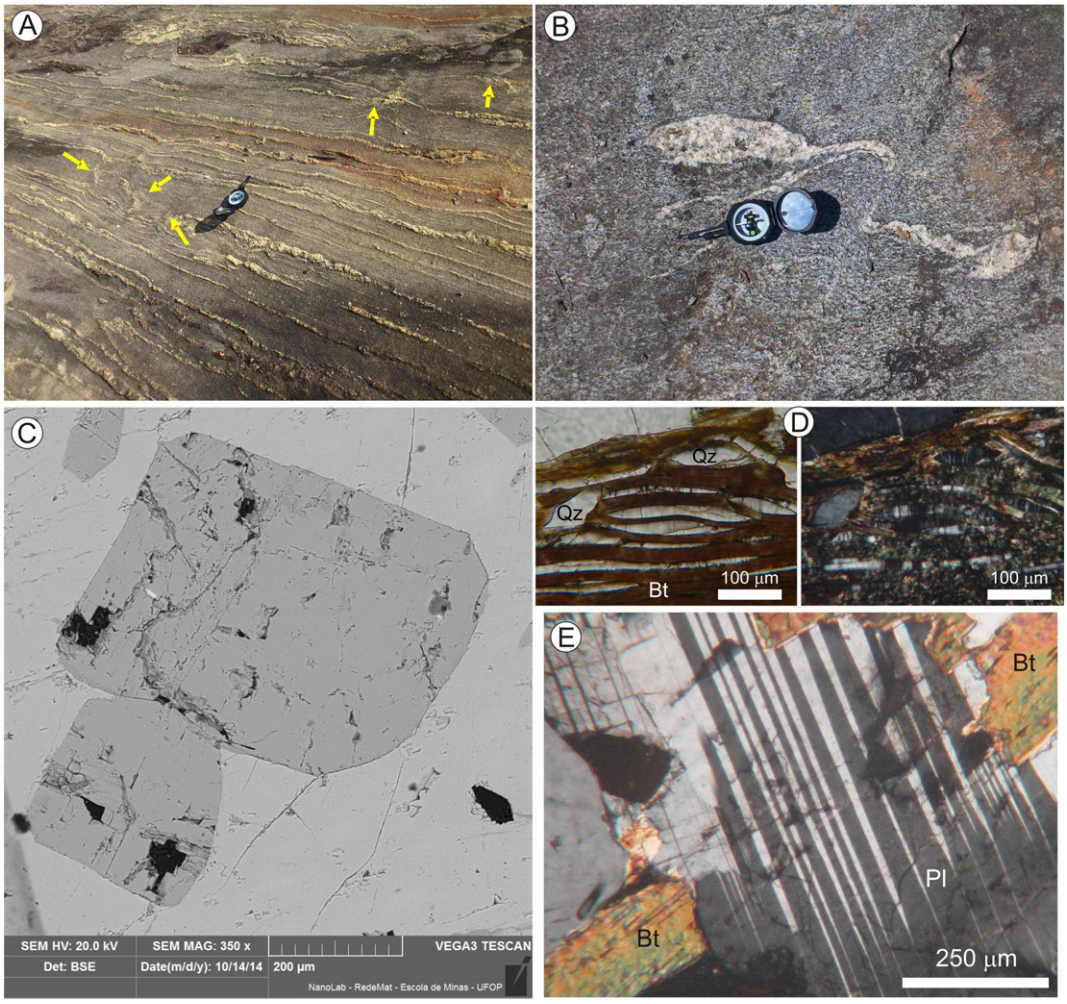

Fig. 3. Petrographic characteristics of the studied G1 granitoids. A–B) Partially molten features preserved in the G1 rocks (samples LG59 and LG63, respectively). Arrows indicate diffuse neosomes likely formed at the end of regional deformation; C) SEM image of a granitoid sample with well preserved euhedral plagioclase grains (sample LG173); D) Microscopic images of elongated quartz grains showing undulose extinctions (transmitted light in the left and polarized light in the right — sample LG31); E) Mechanical twinning developed in plagioclase crystal from a tonalite belonging to the Rancho Alegre pluton (sample LG63). Symbols refer to quartz (Qz), biotite (Bt) and plagioclase (Pl).

^{175}Lu were simultaneously monitored during each analysis step to allow for correction of isobaric interferences of Lu and Yb isotopes on mass 176. The ^{176}Yb and ^{176}Lu were calculated using a ^{176}Yb/^{173}Yb of 0.796218 (Chu et al., 2002) and ^{176}Lu/^{175}Lu of 0.02658 (JWG in-house value). The correction for instrumental mass bias utilized an exponential law and a ^{179}Hf/^{177}Hf value of 0.7325 (Patchett and Tatsumoto, 1980) for correction of Hf isotopic ratios. The mass bias of Yb isotopes generally differs slightly from that of the Hf isotopes with a typical offset of the βHf/βYb of ca. 1.04 to 1.06 when using the ^{172}Yb/^{173}Yb value of 1.35274 from Chu et al. (2002). This offset was determined for each analytical session by averaging the βHf/βYb of multiple analyses of the JMC 475 solution doped with variable Yb amounts and all laser ablation analyses (typically n > 50) of TEMORA zircon with a ^{173}Yb signal intensity of >60 mV. The mass bias behavior of Lu was assumed to follow that of Yb. The Yb and Lu isotopic ratios were corrected using the βHf of the individual integration steps (n = 60) of each analysis divided by the average offset factor of the complete analytical session. In the course of analysis, secondary standards such as Plešovice, TEMORA, 91500, GJ1, and BB9 yielded ^{176}Hf/^{177}Hf ratios of 0.282477 ± 0.000015 (2σ, n = 22), 0.282657 ± 0.000017 (2σ, n = 23), 0.281663 ± 0.000016 (2σ, n = 21), 0.282006 ± 0.000015 (2σ, n = 3), and 0.282298 ± 0.000023 (2σ, n = 10), respectively. These ratios are in good agreement with the recommended values (e.g., Griffin et al., 2006; Wu et al., 2006; Morel et al., 2008; Sláma et al., 2008).

4. Results

4.1. Petrography

The selected samples for detailed petrographic studies were collected in the G1 bodies known as Rancho Alegre, Felizburgo, Pedra do Sino, Bom Jesus da Vitória, São Vítor and Topázio plutons (Fig. 2). The first four plutons, exposed in the central-northeastern sector of the study area, intrude rocks of the Jequitinhonha Complex, whereas the last two cut Rio Doce Group rocks in the southwestern portion of the study area (Fig. 2). These plutons are composed mainly of tonalites, granodiorites and minor monzogranites (Table 1). The dominant lithotypes are light to medium gray, fine to coarse-grained, and consist mostly of plagioclase (33–52%), quartz (23–48%), K-feldspars (10–38%; microcline and orthoclase), biotite (2–25%), and minor hornblende (~3%), the latter mineral being restricted to the Bom Jesus da Vitória pluton. Zircon, apatite, titanite, garnet, epidote, hematite, magnetite and ilmenite are common accessory minerals, while rutile, muscovite, allanite, monazite, pyrrhotite, pyrite and chalcopyrite are restricted to few samples. Muscovite and carbonates are secondary products of plagioclase breakdown. Chlorite occurs as replacement of biotite.

The studied granitoids are, in general, strongly foliated, showing locally migmatitic features (Fig. 3A–B). Undeformed phases also occur, especially in the central portion of the plutons. Preserved igneous features

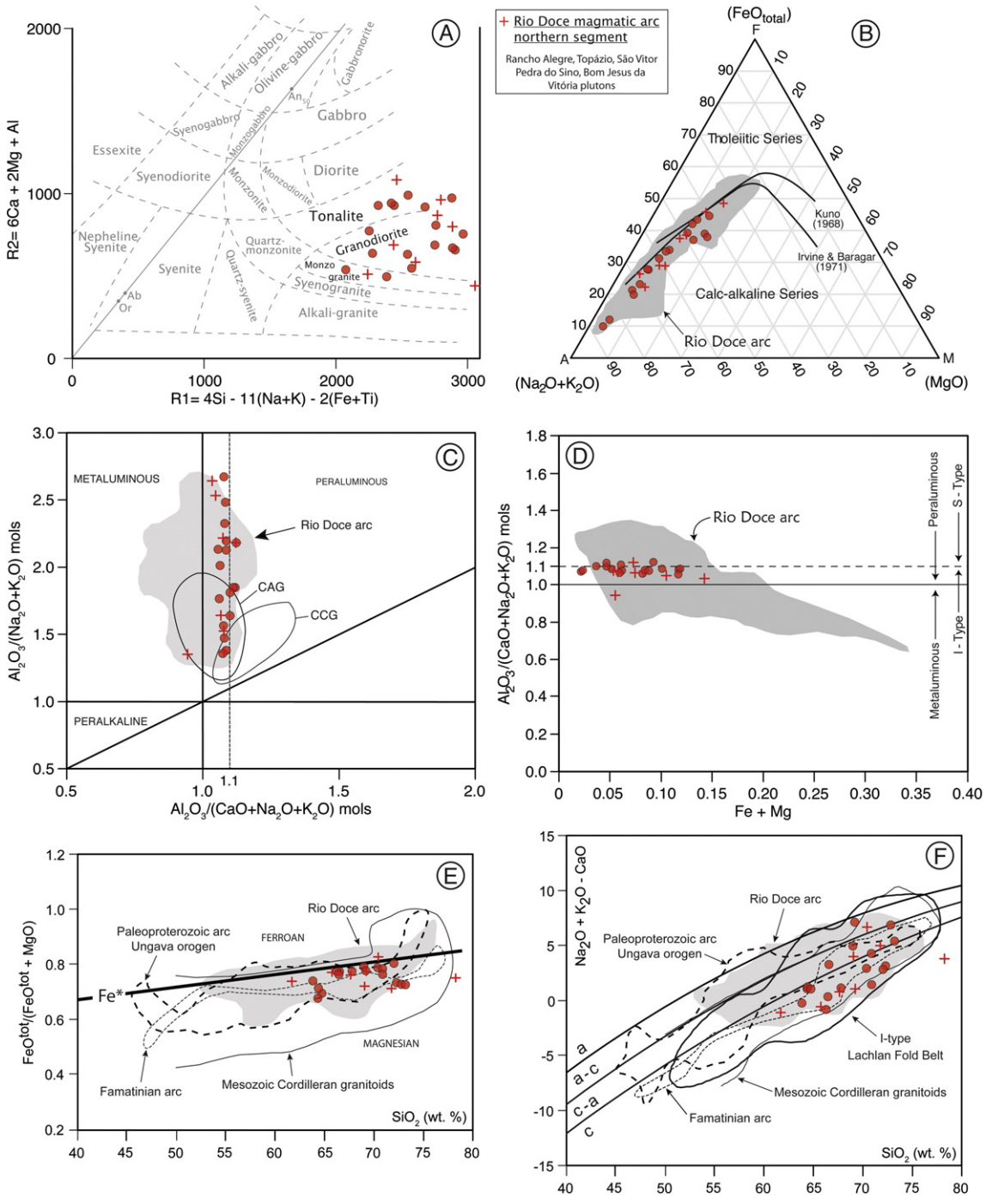

Fig. 4. A) R1–R2 diagram showing the variability of G1 rocks forming the northern segment of the Rio Doce magmatic arc (after De La Roche et al., 1980). Filled circles refer to data of Paes et al. (2010) from G1 rocks that are exposed in the study area, while plus sign represent the analyses of this study. Ab = albite; An_{50} = plagioclase An_{50}; Or = orthoclase. B) AFM diagram showing the distribution of the studied G1 rocks, which is similar to a typical calc-alkaline series (after Rickwood, 1989). C) Characteristics of the rocks forming the northern portion of the Rio Doce arc based on Sand's index (after Maniar and Picolli, 1989). CAG = continental arc granitoids; CCG = continental collision granitoids (see Maniar and Picolli (1989) and references therein for data source). Dashed line marks the transition between I- and S-type granites according to Chappell and White (1974). D) Variation of the Aluminum Saturation Index (A/CNK = mol. $Al_2O_3/CaO + Na_2O + K_2O$) versus maficity (Fe + Mg) for the studied G1 Supersuite granitoids. I/S-type granitoid boundary at ASI = 1.1 from Chappell and White (1974). E) $FeO^{tot}/(FeO^{tot} + MgO)$ versus weight percent SiO_2 diagram showing the predominant magnesian character of the rocks forming the studied G1 Rio Doce arc rocks. Continuous line marks the boundary between ferroan and magnesian plutons of Mesozoic batholiths from North America (see Frost et al., 2001 and references therein for details). F) Plot of $Na_2O + K_2O$–CaO (MALI) versus SiO_2 (wt.%) showing the spread distribution of the Rio Doce arc rocks. For comparison Famatinian, Paleoproterozoic, Mesozoic Cordilleran, and 1155 analyses of I-type granitoids from Lachlan Fold Belt of southeastern Australia are also shown (after Frost et al., 2001). Continuous line constrain the composition range of 344 samples from Cordilleran Mesozoic batholiths of North America; Short dashed line constrain composition range of 12 samples from the Ordovician Famatinian magmatic arc (see Pankhurst et al., 1998 for data source); and long dashed line constrain the composition range of 41 samples from the Paleoproterozoic magmatic arc (for source of data see Dunphy and Ludden, 1998), Ungava orogen, Canada (see Frost et al., 2001, and references therein for additional information). In diagrams B to F, shaded gray area corresponds to the compositional range of ca. 200 granitic samples of the central–southern segments of the Rio Doce arc rocks (for source of data see Gonçalves et al., 2014, and Supplementary data — item 1).

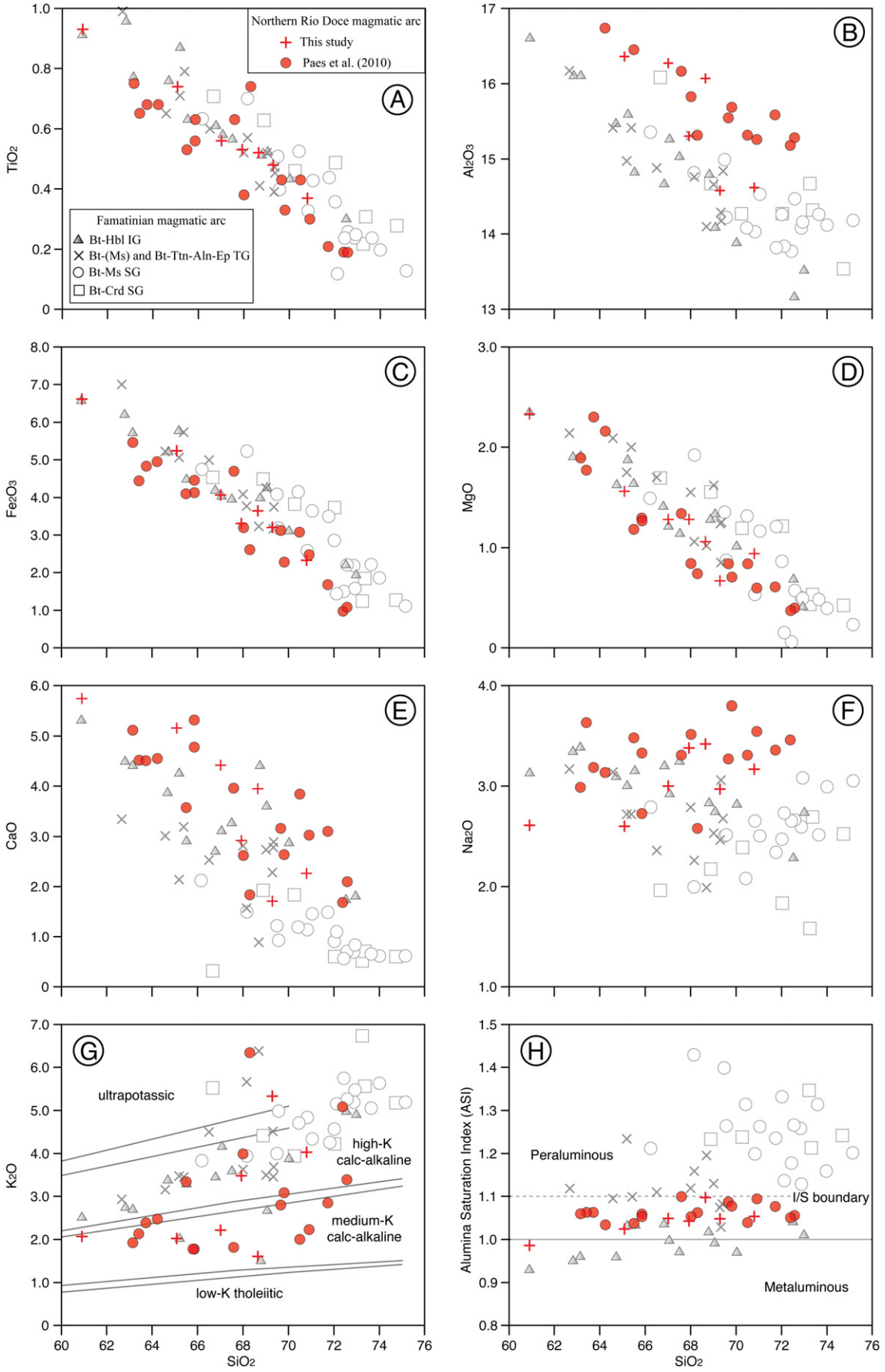
Northern Rio Doce magmatic arc
This study
Paes et al. (2010)
Famatinian magmatic arc
Bt-Hbl IG
Bt-(Ms) and Bt-Ttn-Aln-Ep TG
Bt-Ms SG
Bt-Crd SG
A
B
C
D
E
F
G
H
TiO2
Al2O3
Fe2O3
MgO
CaO
Na2O
K2O
SiO2
ultrapotassic
high-K calc-alkaline
medium-K calc-alkaline
low-K tholeiitic
Alumina Saturation Index (ASI)
Peraluminous
I/S boundary
Metaluminous

such as zoned and tabular plagioclase crystals were observed in Topázio, São Vítor and Pedra do Sino plutons (Fig. 3C). Solid-state deformation features, such as elongated grains, undulose extinctions, mechanical twinning, deformation bands, and occasionally quartz subgrains dominate the texture of the rocks (Fig. 3D–E). The associated metamorphic foliation is marked by the alignment of biotite and hornblende. Brown-reddish biotite is mostly euhedral to subhedral and shows pleochroic halos given by metamictic zircon and monazite grains. Hornblende grains occur as anhedral to subhedral crystals.

4.2. Geochemistry

Eight samples of G1 Supersuite rocks were analyzed for major and trace elements (Supplementary data — item 1). Additional major and trace element compositions of 17 samples from the study area analyzed by Paes et al. (2010) are also shown in the diagrams of Fig. 4. For comparison, we also plotted approximately 200 chemical analyses of granitic rocks belonging to the central–southern portions of the Rio Doce arc (shaded areas in the diagrams of Fig. 4) (see Gonçalves et al., 2014 for data source), 50 chemical compositions of samples from Grosse et al. (2011), mainly for major element comparisons, and 12 from Pankhurst et al. (1998), mainly for trace element comparisons, belonging to the Famatinian magmatic arc, which show similar lithochemical attributes when compared with the Rio Doce magmatic arc (Fig. 5).

The analyses of this study and those of Paes et al. (2010) show a range of compositions from tonalite to monzogranite. Granodiorite (52%) and tonalite (32%) represent by far the most common rocks (Fig. 4A). They have a SiO_2 content ranging from 61.66% to 78.27% (see Supplementary data — item 1 and Paes et al., 2010). The sample compositions are quite homogenous, defining a calc-alkaline series (Fig. 4B), with a dominant peraluminous affinity (average ASI = 1.07), with the exception of sample LG257 (ASI = 0.94) (Fig. 4C–D). All samples are magnesian, except sample LG259 which is ferroan (Fig. 4E), and range from calcic to alkali-calcic. Calcic (68%) and calc-alkaline (24%) rocks form the bulk of the G1 bodies in the study area (Fig. 4F).

The samples show a clear negative correlation between TiO_2, Al_2O_3, Fe_2O_3 and MgO with SiO_2, and although more scattered, CaO (1.84–5.81 wt.%) data also show a slightly negative correlation with SiO_2 (Fig. 5A–E), suggesting fractionation of mafic minerals. On the other hand, a slightly positive correlation between SiO_2 and Na_2O is observed (Fig. 5F). No clear correlation is observed between SiO_2 and K_2O, although K_2O generally increases with SiO_2 (Fig. 5G). The Alumina Saturation Index does not show correlation with SiO_2 (Fig. 5H).

The analyzed samples display REE patterns characterized by enrichment in light rare earth elements (LREE) over heavy rare earth elements (HREE), with $(La/Yb)_N$ ratios ranging between ~11 and ~63 (Supplementary data — item 1, Fig. 6). All samples record a negative Eu anomaly, with Eu/Eu* ratios ranging from ~0.33 to ~0.79 (Supplementary data — item 1). In Primitive Mantle-normalized incompatible element spidergrams (Fig. 7A–D), the G1 rocks show overall large ion lithophile elements (LILE)-enriched patterns (Rb, Th), with values between 100 and 600 times higher than the Primitive Mantle values (Sun and McDonough, 1989). This pattern combined with positive Th, La, Ce, P and Zr anomalies suggests important crustal sourcing. Other common chemical characteristic of the analyzed rocks is the negative Nb, Ta, Sr and Ti anomalies (Fig. 7B), which is normally referred to as an "arc-like signature" (see Niu et al., 2013, and references therein for details).

4.3. Geochronology

Age determinations were performed on 10 rock samples (Figs. 2, 8–10): 7 samples from the G1 Supersuite; 2 samples from the G2 Supersuite; and 1 sample from the G5 Supersuite. The analyzed samples correspond to one enderbite, one tonalite, seven granodiorites, and one syenogranite. A summary of the main features of the dated samples are shown in Tables 2 and 3 and Figs. 8 to 10.

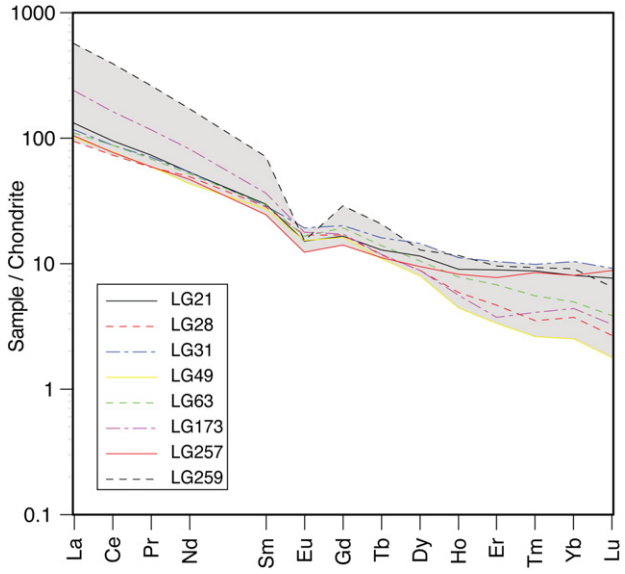

Fig. 6. Rare earth elements diagram normalized by chondrite, according to values of Nakamura (1974). Shadow area delimits the REE concentration for data from this study. See text for further details.

4.3.1. G1 Supersuite (samples LG21, LG27, LG28, LG31, LG49, LG63, and LG173)

The studied G1 Supersuite plutons showed that six samples (LG21, LG27, LG28, LG49, LG63 and LG173) have zircon grains with inherited cores on CL images (Fig. 9). Attempts to date these cores failed and no coherent age data could be obtained, however apparent ages (from 958 Ma to 2574 Ma) are suggestive of inheritance from rocks of the Jequitinhonha Complex (e.g., Gonçalves-Dias et al., 2011). Three samples (LG21, LG31 and LG173) gave ages of 574 ± 7 Ma, 575 ± 6 Ma, and 584 ± 13 Ma, respectively, which are interpreted as their crystallization ages (Fig. 10A, D, G and Tables 2 and 3). On the other hand, four samples (LG27, LG28, LG49 and LG63) have zircon grains, which were divided in two populations, giving ages of ca. 618–595 Ma for crystallization (Fig. 10B-I, C-I, E-I, F-I and Tables 2 and 3) and ca. 555–589 Ma for overgrowths or new crystallized zircon grains (Fig. 10B-II, C-II, E-II, F-II and Tables 2 and 3) interpreted as a migmatization event affecting the rocks. Assuming that this interpretation is correct, the obtained results more likely reflect the regional metamorphic event that took place in the Araçuaí orogen between 590 Ma to 545 Ma, peaking at 575 Ma (Pedrosa-Soares et al., 2001, 2011; Silva et al., 2011; Gradim et al., 2014; Peixoto et al., 2015).

4.3.2. G2 Supersuite (samples LG12 and LG161)

The zircon grains extracted from sample LG12 (Caraí pluton) comprise mainly short-prismatic, and minor elongated grains (up to 422 μm) with length/width ratios in average of 4:1, although higher ratios up to 6:1 can be observed. The axes of zircon grains range from 37 μm to 422 μm. Most grains are dark-gray and some display magmatic oscillatory zoning with inherited cores on CL images (Fig. 9). Several attempts to date these cores were unsuccessful due to the high level of discordance, although apparent ages ranging mainly from ca. 800 Ma to 1200 Ma could be observed. Most zircon grains have Th/U ratios

Fig. 5. A–H) Harker major oxides variation diagrams for the studied G1 rocks and Famatinian arc granitoids from Sierra de Velasco (Grosse et al., 2011). Fields in the K_2O vs. SiO_2 diagram are from Rickwood (1989). I/S-type granitoid boundary at ASI = 1.1 from Chappell and White (1974). IG = I-type granitoids; TG = transitional granitoids; SG = S-type granitoids. Bt = biotite; Hbl = hornblende; Ms = muscovite; Ttn = titanite; Aln = aluminosilicates; Ep = epidote; Crd = cordierite.

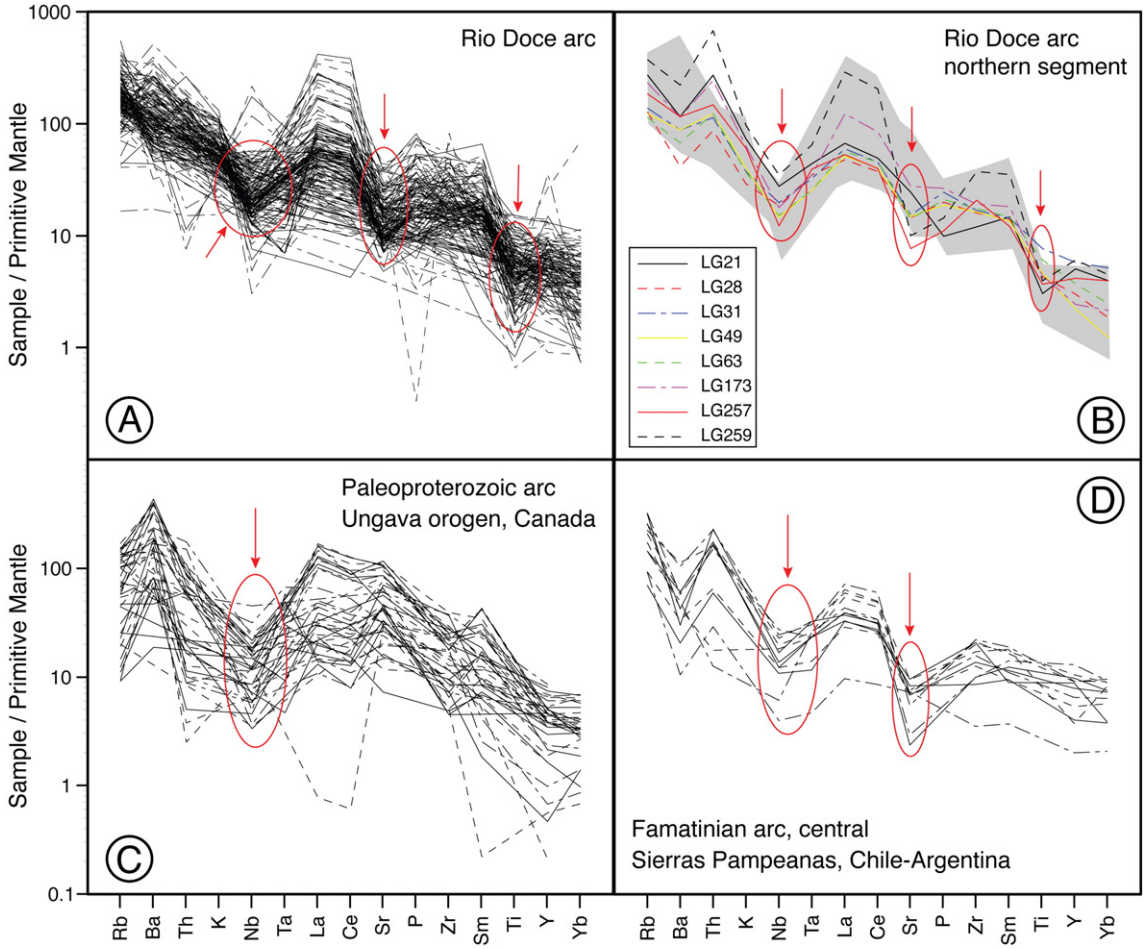

Fig. 7. Multi-element spidergrams normalized to the Primitive Mantle (normalizing values after McDonough and Sun, 1995) of the (A) central–southern G1 Supersuite granites (see Gonçalves et al., 2014 for data source); (B) Studied northern G1 Supersuite rocks. Shadow area delimits the granitoid compositions studied by Paes et al. (2010); (C) Granitoid rocks of the Paleoproterozoic magmatic arc from the Ungava orogen (see Dunphy and Ludden, 1998 for data source), and (D) Granitoid compositions from the Famatinian magmatic arc (see Pankhurst et al., 1998 for data source).

ranging from 0.10 to 0.83 (Supplementary data — item 2). Thirteen concordant to near-concordant (<4% disc.) spot analyses from 12 zircon grains yielded a concordia age of 538 ± 8 Ma (MSWD = 0.21) (Fig. 10H). This age is interpreted as the best approximation of the crystallization age of this sample.

Sample LG161 (Wolff pluton) contains short- and long-prismatic zircon grains, with length/width ratios in average of 4:1, although higher ratios up to 6:1 are observed. The axes of zircon grains range from 47 μm to 330 μm. They are light-gray and some grains display magmatic oscillatory zoning with inherited cores on CL images (Fig. 9). Attempts to obtain ages from these cores failed due to the high level of discordance, although apparent ages mainly between ~960 Ma and ~2000 Ma are found. Four zircon grains have Th/U ratios between 0.38 and 1.22, while two other grains have Th/U ratios of 0.02 and 0.03 (Supplementary data — item 2). Six concordant to near-concordant spot analyses obtained in the same number of zircon grains yielded a concordia age of 563 ± 9 Ma (MSWD = 0.54) (Fig. 10I). We interpret this age as the magmatic crystallization age of this sample.

4.3.3. G5 Supersuite (sample LG29)

The zircon grains extracted from sample LG29 (Fazenda Liberdade pluton) consist of predominantly short-prismatic grains, with length/width ratios in average of 2.6:1, although higher ratios up to 5:1 are observed. The axes of zircon grains range from 45 μm to 245 μm. Most grains are light-gray, and seldom display magmatic oscillatory zoning with no inherited cores on CL images (Fig. 9). Many zircon grains have Th/U ratios higher than 1 (Supplementary data — item 2). Thirty one concordant (<2% disc.; except one grain with 4% disc.) spot analyses obtained in the same number of zircon grains yielded a concordia age of 526 ± 5 Ma (MSWD = 0.12) (Fig. 10J). This age is interpreted as the best approximation of the crystallization age of this sample.

4.4. Rb–Sr and Sm–Nd isotope data

Six whole-rock samples of the G1 Supersuite granitoids were analyzed for Rb–Sr and Sm–Nd isotopes (Supplementary data — item 3). They comprise 4 granodiorites (samples LG21, LG28, LG49 and LG173), 1 tonalite (sample LG63), and 1 enderbite (sample LG31).

The $^{87}Sr/^{86}Sr$ isotopic ratios, when calculated to their crystallization age (ca. 630–580 Ma), range from 0.7059 to 0.7121 (Fig. 11). The $^{87}Rb/^{86}Sr$ ratios vary between 0.6979 and 0.9697 (Supplementary data — item 3). The high $^{87}Sr/^{86}Sr$ ratios and the lack of correlation with the $^{87}Rb/^{86}Sr$ ratios suggest involvement of metasedimentary material in the source of the G1 rocks by variable degrees of melting-assimilation.

The measured $^{143}Nd/^{144}Nd$ ratios are quite homogeneous and show a range of data between 0.511904 and 0.511983. Similarly, the measured $^{147}Sm/^{144}Nd$ ratios are uniform and have values ranging between 0.081 and 0.117 (Supplementary data — item 3). The $\varepsilon_{Nd(i)}$ values, calculated for the crystallization age of the studied rocks, vary between −5.7 and −7.8 (Supplementary data — item 3; Fig. 11). The distribution of T_{DM} model ages spans mainly from 1.36 Ga to 1.68 Ga, showing that Statherian to Calymmian rocks of the Jequitinhonha Complex might

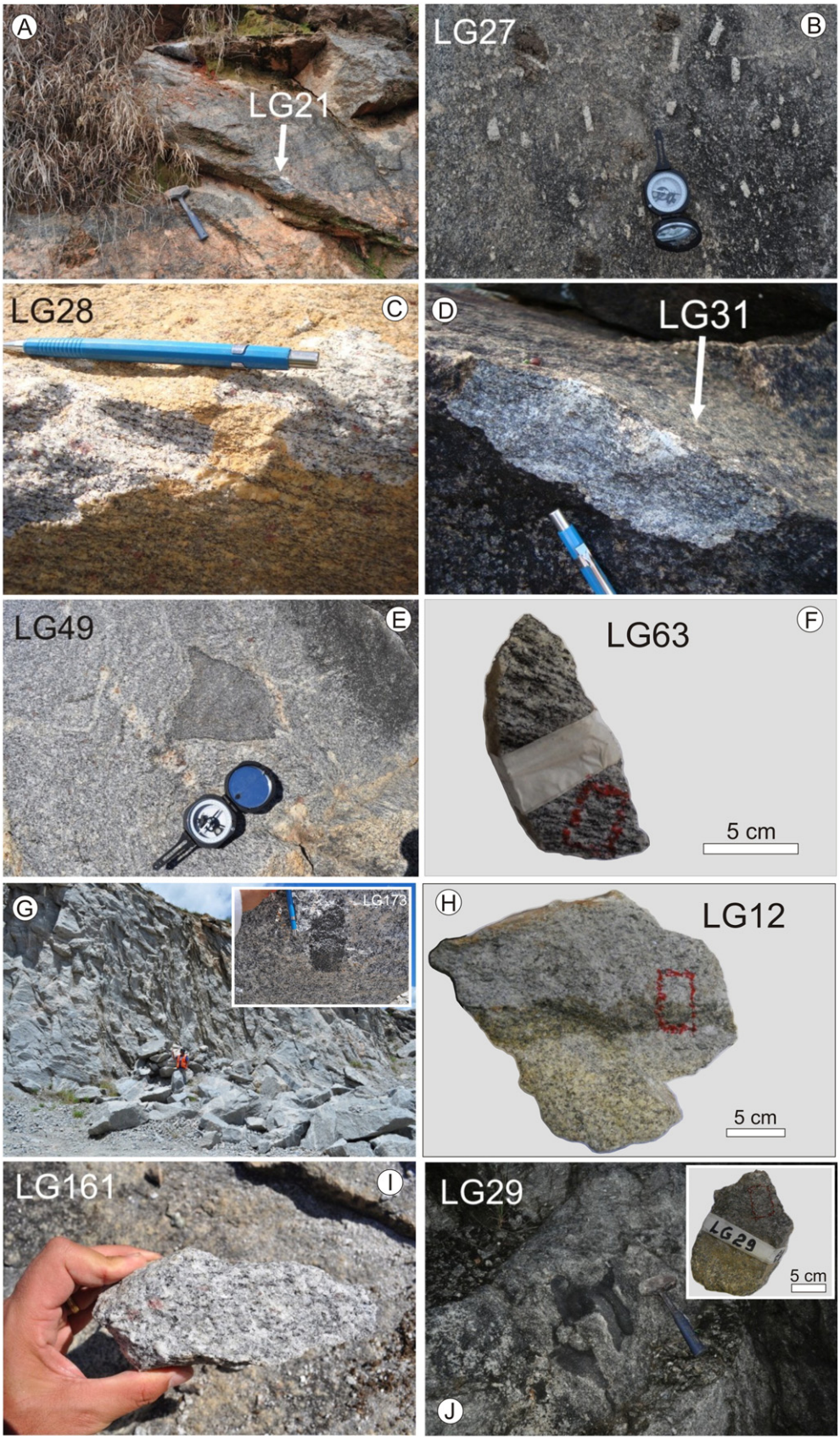

Fig. 8. Macroscopic photographs of the dated samples: A–G) rock samples belonging to the G1 Supersuite; H–I) samples from the G2 Supersuite and J) granitoid sample belonging to the G5 Supersuite (see Fig. 2 for sample location and text for further details).

be involved somehow in the formation of the northern segment of the Rio Doce magmatic arc.

4.5. Lu–Hf isotope data

Four representative samples of the G1 Supersuite were chosen for Hf isotope analyses (see Fig. 2 for sample locality). Taken together, the analyzed zircon grains (9 spots in the sample LG21, 16 in the sample LG27, 22 in the sample LG31 and 22 spots in the sample LG49) have quite homogeneous Hf isotopic compositions, with $^{176}Hf/^{177}Hf$ ratios ranging from 0.282083 to 0.282278 and $\varepsilon_{Hf}(t)$ values from −5.2 to −11.7 (average of −7.1) (Supplementary data — item 4, and Fig. 12).

Zircon grains from the granodiorite belonging to the Topázio pluton (sample LG21, Fig. 2) have $^{176}Hf/^{177}Hf$ ratios of 0.282239–0.282278 and $\varepsilon_{Hf}(t)$ values from −5.2 to −6.5, with average of −6.0 (Supplementary data — item 4). The two distinct groups of previously described zircon grains (Section 4.3.1) from the Pedra do Sino Granodiorite (sample LG27, Fig. 2, Table 3) show quite homogeneous Hf isotopic compositions, with $^{176}Hf/^{177}Hf$ ratios ranging from 0.282144 to 0.282277 and $\varepsilon_{Hf}(t)$ values from −5.5 to −10.2, and average of −7.4 (Supplementary data — item 4). Zircon grains from the enderbite belonging to the Bom Jesus da Vitória pluton (sample LG31, Fig. 2, Table 3) have $^{176}Hf/^{177}Hf$ ratios ranging between 0.282158 and 0.282246, with $\varepsilon_{Hf}(t)$ values from −6.1 to −9.3, and average of −7.7 (Supplementary data — item 4). Similarly to the sample of the Pedra do Sino Pluton (LG27), the two zircon populations from the Rancho Alegre pluton (Fig. 2, Table 3) granodiorite (sample LG49) exhibit quite homogeneous Hf isotopic compositions, with no clear difference among the various zircon grains. Zircon grains from this sample yielded $^{176}Hf/^{177}Hf$ ratios from 0.282083 to 0.282258, with $\varepsilon_{Hf}(t)$ values ranging from −5.4 to −11.7, with average of −7.2 (Supplementary data — item 4, and Fig. 12).

5. Discussion

The rocks of the G1 Supersuite that represent the termination of the Rio Doce magmatic arc in the northern Araçuaí orogen seem to characterize a special assemblage of granitoids. Our results indicate that their crystallization ages range from ca. 630 Ma to 570 Ma (within errors), predating (with some overlap) the ages of typical collisional, peraluminous (ASI > 1.1) granites of the G2 Supersuite, dated between 590 Ma and 545 Ma (e.g., Pedrosa-Soares et al., 2011; Gradim et al., 2014). The obtained ages from this study are in good agreement with previous ages determined for the Rio Doce arc (e.g., Pedrosa-Soares et al., 2011; Gonçalves et al., 2014 and references therein). The G2 Supersuite rocks share similarities with typical collisional granitoids. Consisting mainly of S-type peraluminous two-mica granites and biotite–garnet–cordierite–sillimanite leucogranites, exhibiting chemical patterns of calc-alkaline to alkali-calcic and high-K granitoids, the G2 Supersuite greatly differs from the studied G1 rocks (see Gradim et al., 2014 for a synthesis review on the collisional granitoids from the Araçuaí orogen).

The U–Pb ages obtained in this study for the G1 Supersuite characterizes two rock groups: *i*) older granitoids crystallized between 590 and 630 Ma and migmatized at ca. 585 Ma; *ii*) younger granitoids

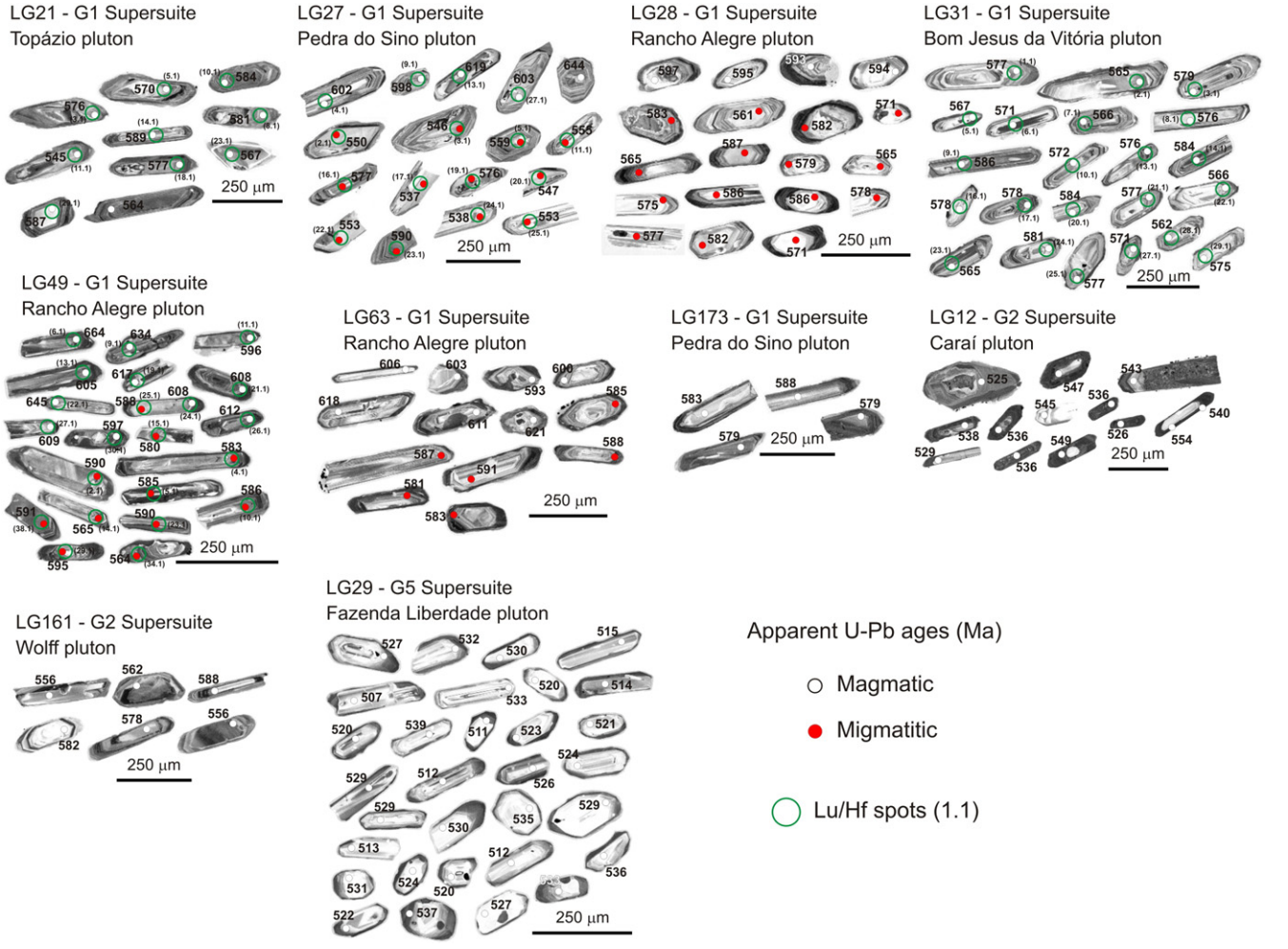

Fig. 9. Cathodoluminescence images showing the external characteristics and internal structures of zircon grains extracted from: G1 Supersuite (samples LG21, LG27, LG28, LG31, LG49, LG63, and LG173); G2 Supersuite (samples LG12 and LG161), and G5 Supersuite (sample LG29). Spot sizes: 25 µm (U–Pb analyses) and 50 µm (Lu–Hf analyses).

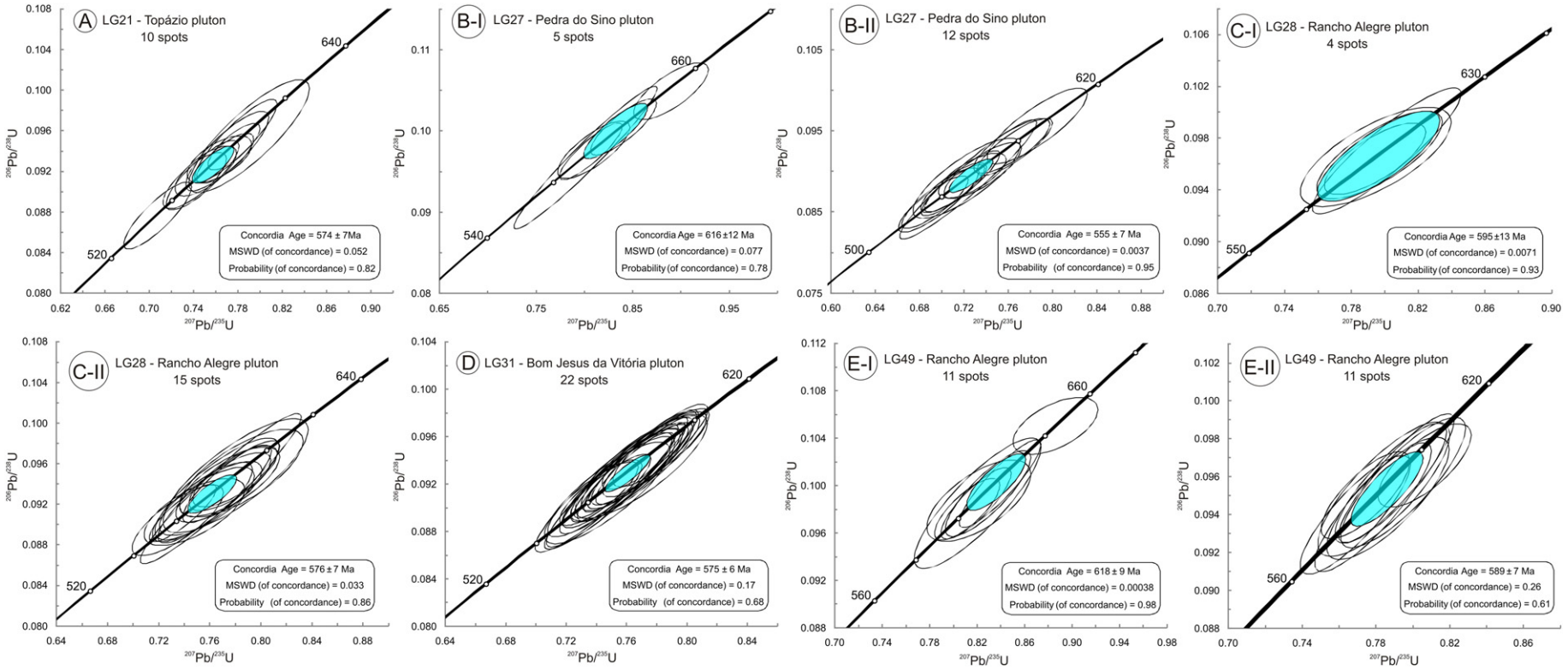

Fig. 10. U–Pb concordia diagrams of LA–MC–ICP–MS analyses of zircon from G1 Supersuite: A–G) samples LG21, LG27, LG28, LG31, LG49, LG63, and LG173; G2 Supersuite: samples LG12 and LG161 (H–I), and G5 Supersuite: sample LG29 (J).

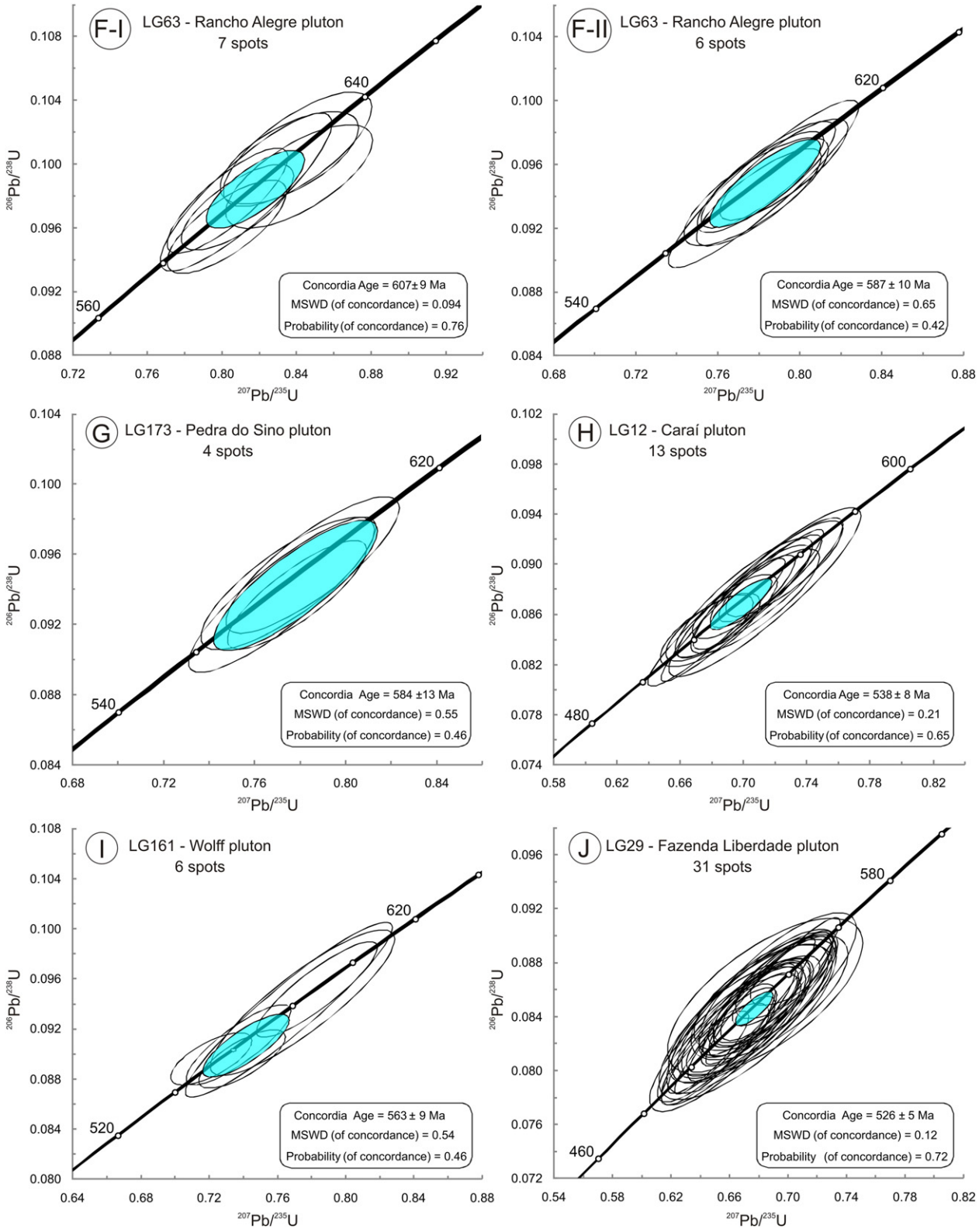

crystallized between 570 and 590 Ma that do not show any evidence for migmatization. The first group of granitoids, exposed in the northernmost extremity of the arc and intruding the Jequitinhonha Complex rocks (Fig. 2), includes the Pedra do Sino and Rancho Alegre plutons (samples LG27, LG28, LG49, and LG63). The close association with the water-rich Jequitinhonha rocks could be responsible for triggering the migmatization of the granitoids in the area.

The second group is exposed in the southwestern (sample LG21) and northeastern (samples LG31 and LG173) portions of the study area and includes the Topázio, Pedra do Sino and Bom Jesus da Vitória plutons.

Table 2
Summary of the main features of the dated samples.

	Pluton (sample)	UTM location	Rock	Mineralogy		Field observations	Age and error (Ma) (MSWD)	
				Main minerals	Accessory-secondary minerals		Magmatic	Migmatitic
G1 Supersuite	Topázio (LG21)	246496/8046722	Granodiorite	Plagioclase, quartz, K-feldspar (mostly microcline), and biotite	Zircon, apatite, hematite, ilmenite	Grayish, medium- to coarse-grained; foliated to banded	574 ± 7 (0.052)	–
	Pedra do Sino (LG27)	294499/8102392	Granodiorite	Plagioclase, quartz, K-feldspar, and biotite	Zircon, monazite, hematite, minor pyrrhotite, chalcopyrite, muscovite and carbonates	Grayish, fine- to coarse-grained; mm- to cm-sized oriented K-feldspars are indicative of magmatic flow; migmatized	616 ± 12 (0.077)	555 ± 7 (0.0037)
	Rancho Alegre (LG28)	295463/8131093	Granodiorite	Plagioclase, quartz, K-feldspar, and biotite	Garnet, zircon and muscovite	Grayish, mostly medium-grained; foliated and migmatized	595 ± 13 (0.0071)	576 ± 7 (0.033)
	Bom Jesus da Vitória (LG31)	327321/8138883	Enderbite	Orthopyroxene, biotite, hornblende, plagioclase, and quartz	Zircon, epidote, allanite, apatite, and minor hematite, ilmenite, chalcopyrite, pyrrhotite and pyrite	Greenish foliated; fine to medium-grained	575 ± 6 (0.17)	–
	Rancho Alegre (LG49)	306086/8145456	Granodiorite	Plagioclase, quartz, K-feldspar, and biotite	Garnet, titanite, apatite, zircon and muscovite	Grayish, mostly medium-grained; foliated and migmatized	618 ± 9 (0.00038)	589 ± 7 (0.26)
	Rancho Alegre (LG63)	296620/8138129	Tonalite	Plagioclase, quartz, K-feldspar (mostly orthoclase), and biotite	Apatite, titanite, zircon and muscovite	Grayish, fine- to coarse-grained; foliated and migmatized	607 ± 9 (0.094)	587 ± 10 (0.65)
	Pedra do Sino (LG173)	318559/8111399	Granodiorite	Plagioclase, quartz, K-feldspar (mostly microcline), and biotite	Apatite, zircon, magnetite, hematite, carbonates and muscovite	Grayish, medium- to coarse-grained; isotropic to strongly foliated with development of shear zones	584 ± 13 (0.55)	–
G2 Supersuite	Caraí (LG12)	193612/8026021	Syenogranite	Plagioclase, microcline, quartz and biotite	Cordierite, garnet, zircon, hematite, muscovite, carbonates and chlorite	Grayish, medium- to coarse-grained; slightly foliated to banded	538 ± 8 (0.21)	539 ± 11 (0.24)
	Wolff (LG161)	278324/8091036	Granodiorite	Plagioclase, quartz, K-feldspar (mostly orthoclase), and biotite	Apatite, garnet, zircon, hematite, ilmenite, cordierite, sillimanite, carbonates and muscovite	Grayish, medium- to coarse-grained; slightly foliated	563 ± 9 (0.54)	–
G5 Supersuite	Fazenda Liberdade (LG29)	294908/8136533	Granodiorite	Plagioclase, quartz, K-feldspar (mostly microcline), and biotite	Apatite, titanite, epidote, rutile, zircon, magnetite, ilmenite, carbonates and muscovite	Grayish, medium- to coarse-grained; isotropic with rounded cm- to decimetric-sized mafic enclaves; feldspar crystals mark a magmatic flow	526 ± 5 (0.12)	–

The Topázio pluton intrudes the metasedimentary rocks of the Rio Doce Group (Fig. 2). Sample LG21 was collected in the central part of the pluton and do not show evidence for migmatization. The age of 574 ± 7 Ma yielded by this sample is among the youngest ages obtained for the G1 magmatism in the Araçuaí orogen (e.g., Pedrosa-Soares et al., 2011; Gonçalves et al., 2014, and references therein). In addition, this age matches quite well, within errors, with the crystallization ages of plutons exposed nearby: the São Vítor (585 ± 7 Ma, Mondou et al., 2012), Brasilândia (581 ± 11 Ma, Tedeschi, 2013), and Guarataia plutons (576 ± 9 Ma, Tedeschi, 2013) also ascribed to the G1 Supersuite (e.g., Pedrosa-Soares et al., 2011; Gonçalves et al., 2014).

Sample LG173 (ca. 585 Ma) from the Pedra do Sino pluton exposed in the northeastern sector of the studied area (Fig. 2) does not show evidence for migmatization (Table 2). The absence for migmatization could be due to lower contents of fertile minerals when compared to sample LG27, extracted in the same region (Fig. 2). This also occurs with sample LG31 (ca. 575 Ma). In this case, the absence of migmatization could be caused by the enderbitic composition of the Bom Jesus da Vitória pluton, requiring higher P–T conditions for the partial melting process. Worth noting, the crystallization age of this sample is similar to other crystallization ages already obtained for Opx-bearing rocks belonging to the Rio Doce magmatic arc (Mondou et al., 2012; Tedeschi, 2013; Gonçalves et al., 2014).

Chemically, the investigated G1 Supersuite rocks correspond to a magnesian, slightly peraluminous, calcic- to calc-alkaline, medium- to high-K acid–silicic series (Figs. 4A–F, and 5G–H). The ε_{Nd} values and initial $^{87}Sr/^{86}Sr$ ratios are intermediate between typical I- and S-type granites (Fig. 11). The Hf isotope data indicates a long period of crustal extraction with T_{DM} ages of ca. 1.5–1.6 Ga, and ε_{Hf} values ranging from −5.2 to −11.7, with an average of −7.1 (Fig. 12). Importantly, typical I- and S-type granites are characterized by a large variability in the Hf isotopic system, and show some overlap in their ε_{Hf} values (see Kemp et al., 2007; Villaros et al., 2012 for a comprehensive review). Thus, the Hf isotope results obtained in this study do not bring additional information for classifying the northernmost G1 rocks either as I- or S-type granitoids.

The studied G1 rocks show features that are particular to arc-related granites, which are:

1) They are calcic (68%) and calc-alkaline (24%), with minor alkali-calcic (8%) members, occasionally containing titanite or garnet, but commonly without hornblende (Table 2). Granitoids that contain hornblende (~3%) are similar to G1 granitoids exposed south of the study area (see Gonçalves et al., 2014 for details), and are also chemically similar to I-type granites (e.g., Frost et al., 2001; Chappell et al., 2012; among others).
2) Most granitoids are slightly peraluminous (average ASI = 1.07) (Figs. 4C–D and 5). Their REE patterns are marked by relative LREE enrichment and HREE depletion, producing a concave-up pattern (Fig. 6). They all have moderate negative Eu and Sr anomalies, likely suggesting feldspar fractionation at the source. Significantly, all granitic rocks sampled here display very similar mantle normalized elemental patterns (Fig. 7).
3) In diagrams of SiO_2 content against Fe number (Fe#) (Fig. 4E) and $Na_2O + K_2O$–CaO (Fig. 4F), the granitic rocks plot close to those emplaced in subduction-related environments (i.e., Cordilleran-type granites; see Frost et al., 2001 for more details).

The northernmost G1 rocks show similarities and differences with rocks of the remaining segments of the Rio Doce arc. South of the study area, the G1 Supersuite is composed of large plutons and batholiths of medium- to high-K, calc-alkaline, tonalitic to granitic compositions, and their Opx-bearing equivalents, generally containing abundant mafic and dioritic facies and enclaves (Nalini et al., 2005; Pedrosa-Soares et al., 2011; Gonçalves et al., 2010, 2014). A few mafic to intermediate plutons rich in gabbroic to enderbitic facies are also present (Novo et al., 2010; Tedeschi, 2013; Gonçalves et al., 2014).

Table 3
Summary of the main characteristics of zircon grains from the studied G1 granitic rocks.

Pluton (sample)	Rock	Zircon information					
		Morphology	Size	Internal features	Length/width ratios	Th/U ratios	Observations
Topázio (LG21)	Granodiorite	Short and long prismatic grains	Up to 430 μm	Medium-gray with few grains displaying magmatic oscillatory zoning with inherited cores on CL images	4:1 to 6:1	0.20 to 1.32, with few exceptions close to 0.05	No metamorphic overgrowth
Pedra do Sino (LG27)	Granodiorite	Short-prismatic and rounded grains	55 μm–320 μm	Light to medium-gray with few grains exhibiting magmatic, sometimes chaotic, oscillatory zoning on CL images	3:1 to 4:1	0.20 to 1.76 (first population) 0.15 to 1.19 (second population)	Inherited cores with apparent age of ca. 1070 Ma
Rancho Alegre (LG28)	Granodiorite	Short prismatic grains	50 μm–280 μm, in average < 200 μm	Light to medium-gray with some grains displaying magmatic oscillatory zoning and inherited cores on CL images	2.5:1 to 5:1	0.10 to 0.35 (first population) 0.04 to 0.93 (second population)	Inherited cores with apparent ages from 928 Ma to 2553 Ma
Bom Jesus da Vitória (LG31)	Enderbite	Short and long prismatic grains	47 μm–460 μm	Light-gray with most grains displaying magmatic oscillatory zoning with no inherited cores on CL images	3:1 to 6.5:1	0.23 to 1.15, with one exception of 0.12	Sometimes rounded boundaries, however no metamorphic overgrowth
Rancho Alegre (LG49)	Granodiorite	Short-, long-prismatic and large elongated grains	Up to 345 μm	Medium-gray with some grains displaying magmatic oscillatory zoning and few grains with inherited cores	4:1 to 6:1	0.10 to 0.32 (first population) 0.11 to 1.76 (second population)	Inherited cores with apparent ages of 958 Ma, 1560 Ma and 2405 Ma
Rancho Alegre (LG63)	Tonalite	Long and elongated grains	28 μm–436 μm	Medium-gray with some grains displaying magmatic oscillatory zoning on CL images; few grains have inherited cores and exhibit corroded and rounded boundaries	4:1 to 9:1	0.10 to 1.07 (first population) 0.17 to 0.80 (second population)	Inherited cores with apparent ages of 1283 Ma and 2574 Ma; no metamorphic overgrowth
Pedra do Sino (LG173)	Granodiorite	Short and long prismatic grains	60 μm–310 μm	Medium-gray, show slightly magmatic oscillatory zoning and some grains with inherited cores on CL images	4:1	0.11 to 1.83	Inherited cores with apparent ages of 1091 Ma, 1256 Ma and 2255 Ma

Particularly, they are metaluminous to slightly peraluminous (average ASI = 1.02; obtained from 25 samples studied by Gonçalves et al., 2014), and hornblende–biotite bearing granitoids, while the northernmost G1 rocks are essentially slightly peraluminous (average ASI = 1.07), and mostly biotite-bearing granitoids. The zircon U–Pb crystallization ages of the previously studied G1 Supersuite rocks range predominantly from 630 Ma to 580 Ma, similar to the studied granitoids, but contain large amounts of ca. 2.1 Ga inherited zircon grains that are probably derived from the basement units (Noce et al., 2007; Pedrosa-Soares et al., 2011; Gonçalves et al., 2014). The ca. 2.1 Ga inherited zircon ages were not found in the northernmost G1 rocks. The ε_{Nd} values of the previously studied G1 Supersuite rocks range from −6 to −13. Their initial $^{87}Sr/^{86}Sr$ ratios vary from 0.7088 to 0.7233. The Sm–Nd isotope data indicates a long period of crustal extraction with T_{DM} ages of ca. 1.39–2.26 Ga (Nalini, 1997; De Campos et al., 2004; Martins et al., 2004; Tedeschi, 2013 and references therein). Therefore, the Nd and Sr isotopic results obtained in this study are in good agreement with data from the literature on the Rio Doce arc rocks (Supplementary data — item 3, and Fig. 11).

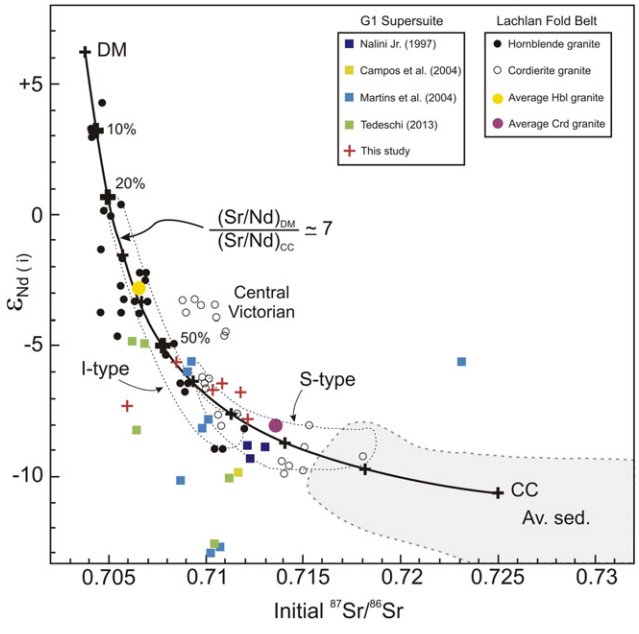

Fig. 11. Epsilon Nd versus Sr/Sr diagram for granitoids from the Rio Doce magmatic arc. DM stands for depleted mantle and CC for the continental crust. The hyperbola represents a putative mixing line between the average Ordovician turbidite (av. sEd.) and the depleted mantle end-member (DM) determined by McCulloch and Chappell (1982), and encapsulates most hornblende and cordierite granites (black crosses represent 10% mixing intervals). Isotopic compositions for granites from the Lachlan fold belt as well as data from G1 granitoids that are exposed south of the studied area are plotted for comparisons (modified from Kemp and Hawkesworth, 2003).

The petrographic, geochemical and isotopic characteristics of the granitic rocks forming the northern end of the Rio Doce arc clearly indicate that they share a series of features with both I-type and S-type granites (cf. Chappell and White, 2001). Furthermore, the lack of hornblende (with the exception of sample LG31, Table 2), the local occurrence of titanite, the peraluminosity affinity and scarcity of muscovite, along with the occurrence of both meta-igneous and metasedimentary enclaves indicate that they are in many aspects similar to the transitional I/S-type granitoids described by Grosse et al. (2011) in the Famatinian magmatic arc of northwestern Argentina. In reality, the studied G1 rocks show features that are intermediate between I-type and the transitional I/S-type granites from the Famatinian magmatic arc (see Grosse et al. 2011).

Using of the A–B diagram of Debon and Le Fort (1983) and Villaseca et al. (1998), the studied G1 rocks plot in distinct fields. The G1 granites are in general moderate to low peraluminous rocks (88% of the samples), and lie between typical I and the I/S-type granites from the Famatinian arc (Fig. 13). In addition, regardless of their felsic or mafic character the G1 granitoids show fairly constant peraluminosity. Indeed, the composition plots of the studied rocks on the A–B diagram generate a trend comparable to experimental melting of greywackes and amphibolites (Fig. 13). This fact suggests that a progressively incorporation of metasedimentary material in the melts result in

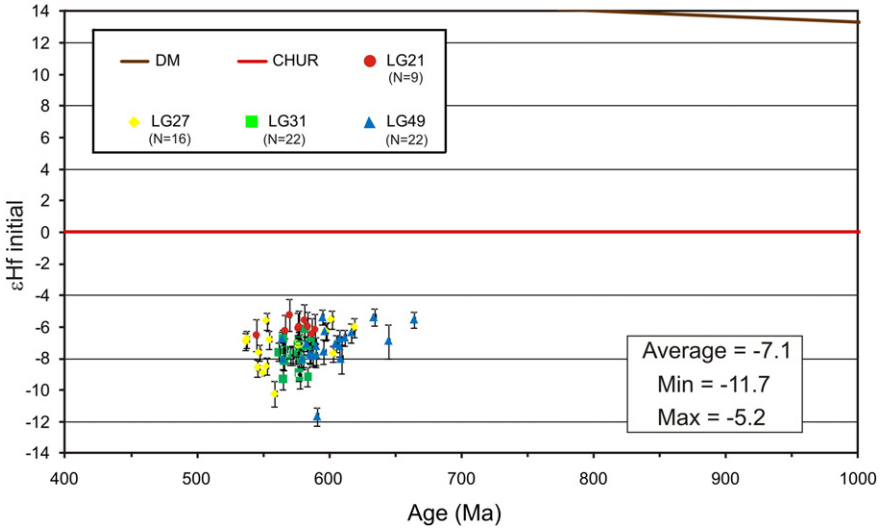

Fig. 12. Hf isotopic composition of zircon grains from the studied granitoids plotted against their ages. DM = depleted mantle; CHUR = chondritic uniform reservoir.

compositional variations between pure I-type rocks and transitional I/S granites. This interpretation is reinforced by negative ε_{Hf} and ε_{Nd} values, ranging between −5.2 and −11.7, T_{DM} ages of ca. 1.5–1.6 Ga, lack of hornblende and strong crustal initial $^{87}Sr/^{86}Sr$ ratios obtained for the studied G1 Supersuite rocks (Supplementary data — items 3 and 4, and Figs. 11, 12, and 13).

Additionally, as shown by the binary diagrams of Fig. 14A–D, the studied granitoids plot almost entirely in the field of dehydration-melting of amphibolites. Only a few samples plot in the fields of dehydration-melting of greywackes and none of them in the felsic or mafic pelite fields, a chemical behavior similar to I- and I/S-type granitoids of the Famatinian magmatic arc (Fig. 14A–D). The higher K/Na ratios exhibit by the studied granitoids in relation to basaltic-amphibolite-derived melts (Fig. 14D) could be attributed to re-melting of older calc-alkaline rocks that were themselves formed by mantle–crust interactions, as postulated by Patiño Douce (1999) and Grosse et al. (2011).

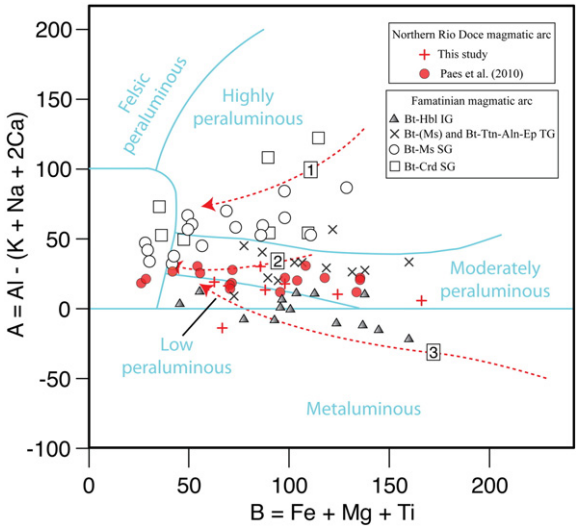

Fig. 13. A–B diagram of Debon and Le Fort (1983) for the studied northernmost Rio Doce arc rocks. Granitoid compositional fields in blue are from Villaseca et al. (1998). Dashed red arrows are trends of experimental melts from different protoliths: 1 = pelite-derived melt (Vielzeuf and Holloway, 1988); 2 = greywacke-derived melt (Conrad et al., 1988); 3 = amphibolite-derived melt (Beard and Lofgren, 1991). Sample symbols are as in Figs. 4 and 5.

Given the regional scenario, we propose that the origin of the studied granitic rocks involved mixing of both dehydration-melting of meta-igneous (amphibolites) rocks and dehydration-melting of metasedimentary (greywackes) rocks. The real contribution of each end-member is, however, a challenging work still to be done. In this context, the involvement of mantle-related magmas seems to be effective as triggering mechanism for the crustal melting process.

5.1. Tectonic implications

In the previous section we made a case for significant recycling of continental crust at the termination of the Rio Doce magmatic arc. The across-arc variation from I- to S-type granites observed in the Famatinian magmatic arc, led Grosse et al. (2011) to interpret a progressive increase in the contribution of metasedimentary material toward the interior of the continent, possibly at progressively higher crustal levels and associated with increasing crustal thickness. They argued in favor of a single and continuous subduction-related setting, in which metaluminous magmas are produced at continental margins, while peraluminous magmas (with minor assimilation of mafic melts) are generated in the continental interior via crustal recycling and substantial melting of metasedimentary rocks. Considering that the Araçuaí–West Congo orogen developed in an uncommon confined environment, involving the closure of a basin that was partially ensialic and partially floored by oceanic crust (Pedrosa-Soares et al., 1992, 1998, 2001, 2008; Alkmim et al., 2006; Queiroga et al., 2007), it is likely that the terminal segment of the Rio Doce arc developed in the almost fully ensialic portion of the basin, with minor influence of oceanic crust subduction and mafic mantle-derived magmas. In this scenario, the increase in the contribution of metasedimentary material must have occurred from south to north, as indicated by the higher peraluminous and transitional I/S-type character of the studied G1 Supersuite granitoids. The tectonic panorama of northern Rio Doce arc is illustrated by the block-diagram of Fig. 15. Nevertheless, participation of metasedimentary material was not sufficient to erase the arc- and subduction-related chemical signatures (e.g., Niu et al., 2013) of the investigated granitoids (e.g., Fig. 7).

6. Conclusions

Field and petrographic observations, along with the results of our geochemical, isotopic and geochronological study of the granitoids

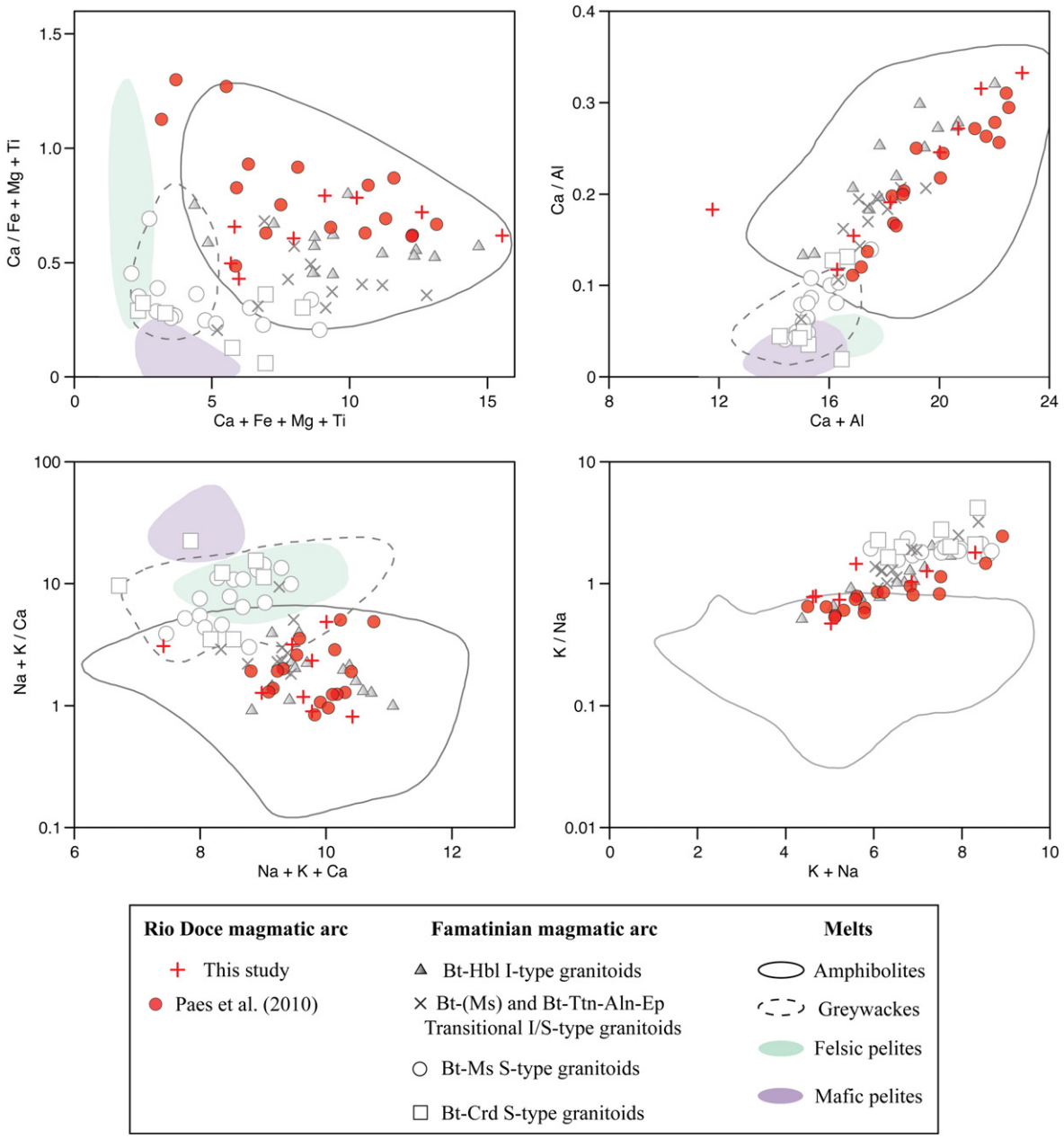

Fig. 14. Major element diagrams modified from Patiño Douce (1999) and Grosse et al. (2011), with compositions of the studied Rio Doce arc rocks and of Famatinian arc granitoids (from Grosse et al., 2011). Fields are compositions of experimental dehydration-melting of different types of rocks (for source of data see Patiño Douce, 1999).

forming the northernmost and almost fully intracontinental segment of the Rio Doce magmatic arc lead to the following conclusions:

1. The terminal segment of the arc consists of partially deformed and migmatized granodiorites, tonalites, and minor monzogranites.
2. Differently from the hornblende–biotite bearing I-type granites (ASI = 1.02) of the central and southern portions of the arc, the northernmost G1 Supersuite granitoids in general do not contain hornblende, are poor in mafic enclaves and exhibit characteristics (e.g., average ASI = 1.07) of both I-type and transitional I/S-type granites (sensu Grosse et al., 2011).
3. Chemically, the granitoids correspond to magnesian, slightly peraluminous, calcic- to calc-alkaline, medium- to high-K acid-silicic rocks, in this respect similar to Cordilleran-type granites described worldwide.
4. The obtained U–Pb zircon ages indicate that terminal branch of the arc developed between 618 Ma and 574 Ma and underwent partial melting between 589 Ma and 555 Ma, in the course of the regional metamorphic event affecting the Araçuaí orogen. Ages obtained in zircon cores suggest significant contribution of the basement and Jequitinhonha Complex rocks in the generation of the northern segment of the arc.
5. The Sr and Nd isotopic composition of the granitoids, combined with Lu–Hf data also point toward a strong involvement of the continental crust in the generation of studied granitoids.
6. Partial melting and mixing of metasedimentary and meta-igneous (amphibolites) rocks were probably the main process involved in the generation of the arc terminal branch. However, further work in key places is required for the evaluation of the crustal and mantle sourcing in the production of the G1 Supersuite of the northern Rio Doce arc.

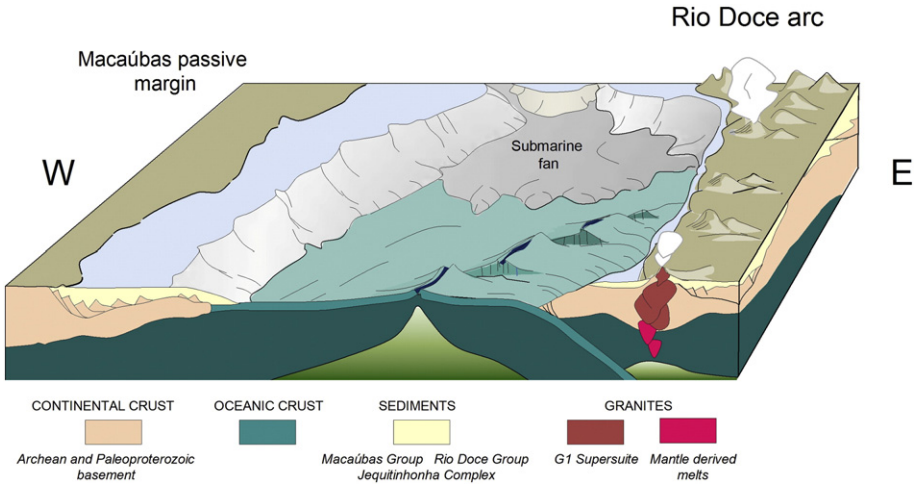

Fig. 15. Block-diagram showing the tectonic setting of the Rio Doce magmatic arc and its terminal segment in the continental domain of the Macaúbas basin, whose closure led to development of the Araçuaí orogen.

Supplementary data to this article can be found online at http://dx.doi.org/10.1016/j.gr.2015.07.015.

Acknowledgments

We are grateful to the Coordenação de Aperfeiçoamento de Pessoal de Nível Superior (CAPES) and Conselho Nacional de Desenvolvimento Científico e Tecnológico (CNPq) for the financial support. We would like to thank Allan Collins for the editorial handling and an anonymous reviewer for the careful corrections and suggestions that greatly improved the manuscript. LG thanks the Prof. Edward Sawyer for helpful comments about migmatitic features. The technical staffs of the CPGeo — University of São Paulo (Maurício de Souza, Vasco dos Loios, and Walter Sproesser), LAGIR — State University of Rio de Janeiro (Carla Neto, Gilberto Vaz, João Barcellos, and Ricardo Travassos), as well as of the NanoLab/RedeMat (Ney Sampaio) are thanked for laboratorial facilities.

References

Alkmim, F.F., Marshak, S., Fonseca, M.A., 2001. Assembling West Gondwana in the Neoproterozoic: clues from the São Francisco Craton region, Brazil. Geology 29, 319–322.

Alkmim, F.F., Marshak, S., Pedrosa-Soares, A.C., Peres, G.G., Cruz, S.C.P., Whittington, A., 2006. Kinematic evolution of the Araçuaí–West Congo orogen in Brazil and Africa: nutcracker tectonics during the Neoproterozoic assembly of Gondwana. Precambrian Research 149, 43–64.

Almeida, F.F.M., Litwinski, N., 1984. Província Mantiqueira: setor setentrional. In: de Almeida, F.F.M., Hasui, Y. (Eds.), O Pré-Cambriano do Brasil. Editora Edgar Blücher, São Paulo, pp. 282–307.

Basei, M.A.S., Brito Neves, B.B., Siga-Junior, O., Babinski, M., Pimentel, M.M., Tassinari, C.C.G., Hollanda, M.H.B., Nutman, A., Cordani, U.G., 2010. Contribution of SHRIMP U–Pb zircon geochronology to unravelling the evolution of Brazilian Neoproterozoic fold belts. Precambrian Research 183, 112–144.

Beard, J.S., Lofgren, G.E., 1991. Dehydration melting and water-saturated melting of basaltic and andesitic greenstones and amphibolites at 1, 3, and 6.9 kbar. Journal of Petrology 32, 365–401.

Brito Neves, B.B., Campos Neto, M.C., Fuck, R., 1999. From Rodinia to Western Gondwana: an approach to the Brasiliano/Pan-African cycle and orogenic collage. Episodes 22, 155–199.

Campos-Neto, M.C., 2000. Orogenic systems from southwestern Gondwana. An approach to Brasiliano–Pan African Cycle and orogenic collage in south eastern Brazil. In: Cordani, U.G., Milani, E.J., Thomaz-filho, A., Campos, D.A. (Eds.), Tectonic Evolution of South America. 31st International Geological Congress, Rio de Janeiro, pp. 335–365.

Carvalho, J.B., Pereira, L.M.M., 2000. Petrografia, Relatório Integrado Etapa 1, folhas SE.24-V, SE.23-Z, SE.24-Y (partes), Estado de Minas Gerais, Escala 1:500,000 (93 p.). In: Projeto Leste, CPRM-CODEMIG (Eds.), Belo Horizonte, pp. 335–365.

Chappell, B.W., White, A.J.R., 1974. Two contrasting granite types. Pacific Geology 8, 173–174.

Chappell, B.W., White, A.J.R., 2001. Two contrasting granite types: 25 years later. Australian Journal of Earth Sciences 48, 489–499.

Chappell, B.W., Colleen, J.B., Doone, W., 2012. Peraluminous I-type granites. Lithos 153, 142–153.

Chemale Jr., F., Kawashita, K., Dussin, I.A., Ávila, J.N., Justino, D., Bertotti, A., 2012. U–Pb zircon in situ dating with LA–MC–ICP–MS using a mixed detector configuration. Anais da Academia Brasileira de Ciências 84, 275–295.

Chu, N.C., Taylor, R.N., Chavagnac, V., Nesbitt, R.W., Boella, R.M., Milton, J.A., German, C.R., Bayon, G., Burton, K., 2002. Hf isotope ratio analysis using multi-collector inductively coupled plasma mass spectrometry: an evaluation of isobaric interference corrections. Journal of Analytical Atomic Spectrometry 17, 1567–1574.

Conrad, W.K., Nicholls, I.A., Wall, V.J., 1988. Water-saturated and undersaturated melting of metaluminous and peraluminous crustal composition at 10 kb: evidence for the origin of silicic magmas in the Taupo Volcanic Zone, New Zealand, and other occurrences. Journal of Petrology 29, 765–803.

Cordani, U.G., D'Agrella-Filho, M.S., Brito Neves, B.B., Trindade, R.I.F., 2003. Tearing up Rodinia: the Neoproterozoic paleogeography of South American cratonic fragments. Terra Nova 15, 350–359.

De Campos, C., Mendes, J., Ludka, I., de Medeiros, S., de Moura, J., Wallfass, C., 2004. A review of the Brasiliano magmatism in southern Espírito Santo, Brazil, with emphasis on post-collisional magmatism. In: Weinberg, R., Trouw, R., Fuck, R., Hackspacher, P. (Eds.), The 750–550 Ma Brasiliano Event of South America. Journal of the Virtual Explorer, Electronic Edition1441-8142 vol. 17 (Paper 1).

De la Roche, H., Leterrier, J., Grande Claude, P., Marchal, M., 1980. A classification of volcanic and plutonics rocks using R1–R2 diagrams and major element analyses — its relationships and current nomenclature. Chemical Geology 29, 183–210.

Debon, F., Le Fort, P., 1983. A chemical–mineralogical classification of common plutonic rocks and associations. Transactions of the Royal Society of Edinburgh: Earth Sciences 73, 135–149.

DePaolo, D.J., 1981. Neodymium isotopes in the Colorado Front Range and implications for crust formation and mantle evolution in the Proterozoic. Nature 291, 193–197.

Dunphy, J.M., Ludden, J.N., 1998. Petrological and geochemical characteristics of a Paleoproterozoic magmatic arc (Narsajuaq terrane, Ungava orogen, Canada) and comparisons to Superior Province granitoids. Precambrian Research 91, 109–142.

Figueiredo, M.C.H., Campos Neto, M.C., 1993. Geochemistry of the Rio Doce magmatic arc, southeastern Brazil. Anais da Academia Brasileira de Ciências 65, 63–81.

Fontes, C.Q., 2000. Folha Águas Formosas. Projeto Leste. CPRM-CODEMIG. http://www.portalgeologia.com.br/mapa/.

Frost, B.R., Arculus, R.J., Barnes, C.G., Collins, W.J., Ellis, D.J., Frost, C.D., 2001. A geochemical classification of granitic rocks. Journal of Petrology 42, 2033–2048.

Gomes, A. C. B., 2008. Projeto Jequitinhonha: Folha Rio do Prado (SE.24-V-A-VI), 1: 100,000. Programa Geologia do Brasil. Belo Horizonte, CPRM.

Gonçalves, L.E. da S., Alkmim, F.F., Pedrosa-Soares, A.C., 2010. Características geoquímicas da Suíte G1, arco magmático do Orógeno Araçuaí, entre Governador Valadares e Ipanema, MG. Revista da Escola de Minas 63, 457–464.

Gonçalves, L., Farina, F., Lana, C., Pedrosa-Soares, A.C., Alkmim, F., Nalini Jr., H.A., 2014. New U–Pb ages and lithochemical attributes of the Ediacaran Rio Doce magmatic arc, Araçuaí confined orogen, southeastern Brazil. Journal of South American Earth Sciences 52, 129–148.

Gonçalves-Dias, T., Pedrosa-Soares, A.C., Dussin, I.A., Alkmim, F.F., Caxito, F.A., Silva, L.C., Noce, C.M., 2011. Maximum sedimentation age and provenance of the Jequitinhonha Complex in the type–area (Araçuaí orogen): first U–Pb (LA–ICP–MS) data from detrital zircon grains. Geonomos 19, 121–130.

Goscombe, B.D., Gray, D.R., 2008. Structure and strain variation at mid-crustal levels in a transpressional orogen: a review of Kaoko Belt structure and the character of West Gondwana amalgamation and dispersal. Gondwana Research 13, 45–85.

Gradim, C., Roncato, J., Pedrosa-Soares, A.C., Cordani, U., Dussin, I., Alkmim, F.F., Queiroga, G., Jacobsohn, T., da Silva, L.C., Babinski, M., 2014. The hot back-arc zone of the Araçuaí orogen, Eastern Brazil: from sedimentation to granite generation. Brazilian Journal of Geology 44 (1), 155–180.

Griffin, W.L., Pearson, N.J., Belousova, E.A., Saeed, A., 2006. Comment: Hf-isotope heterogeneity in zircon 91500. Chemical Geology 233, 358–363.
Grosse, P., Bellos, L.I., de los Hoyos, C.R., Larrovere, M.A., Rossi, J.N., Toselli, A.J., 2011. Across-arc variation of the Famatinian magmatic arc (NW Argentina) exemplified by I-, S- and transitional I/S-type Early Ordovician granitoids of the Sierra de Velasco. J. S. Am. Earth Sci. 32, 110–126.
Heilbron, M., Tupinambá, M., Valeriano, C., Armstrong, R., Eirado-Silva, L.G., Melo, R.S., Simonetti, A., Pedrosa-Soares, A.C., Machado, N., 2013. The Serra da Bolívia Complex: the record of a new Neoproterozoic arc-related unit at Ribeira belt. Precambrian Research 238, 158–175.
Jackson, S.E., Pearson, N.J., Griffin, W.L., Belousova, E.A., 2004. The application of laser ablation–inductively coupled plasma–mass spectrometry to in situ U–Pb zircon geochronology. Chemical Geology 211, 47–69.
Kemp, A.I.S., Hawkesworth, C.H., 2003. Granitic perspectives on the generation and secular evolution of the continental crust. In: Holland, H.D., Turekian, K.K. (Eds.), Treatise on Geochemistry. Elsevier, Amsterdam, pp. 349–431.
Kemp, A.I.S., Hawkesworth, C.J., Foster, G.L., Paterson, B.A., Woodhead, J.D., Hergt, J.M., Gray, C.M., Whitehouse, M.J., 2007. Magmatic and Crustal differentiation history of granitic rocks from Hf—O Isotopes in Zircon. Science 315, 980–983.
Kemp, A.I.S., Hawkesworth, C.J., Paterson, B.A., Kinny, P., 2006. Episodic growth of the Gondwana Supercontinent from hafnium and oxygen isotopes in zircon. Nature 439, 580–583.
Liu, R., Li, J.-W., Bi, S.-J., Hu, H., Chen, M., 2013. Magma mixing revealed from in situ zircon U–Pb–Hf isotope analysis of the Muhuguan granitoid pluton, eastern Qinling orogen, China: implications for late Mesozoic tectonic evolution. International Journal of Earth Sciences (Geologische Rundschau) 102, 1583–1602.
Ludwig, K.R., 2003. Using Isoplot/Ex, version 3.00, a geochronological toolkit for Microsoft Excel. Berkeley Geochronology Center, Special Publication 1 (43 pp.).
Maniar, P.D., Picolli, P.M., 1989. Tectonic discrimination of granitoids. Geological Society of America Bulletin 101, 635–643.
Martins, V.T. de S., Teixeira, W., Noce, C.M., Pedrosa-Soares, A.C., 2004. Sr and Nd characteristics of Brasiliano/Pan-Africano granitoid plutons of the Araçuaí orogen, southeastern Brazil: tectonic implications. Gondwana Research 7, 75–89.
McCulloch, M.T., Chappell, B.W., 1982. Nd isotopic characteristics of S- and I-type granites. Earth and Planetary Science Letters 58, 51–64.
McDonough, W.F., Sun, S.-S., 1995. The composition of the Earth. Chemical Geology 120, 223–253.
Mondou, M., Egydio-Silva, M., Vauchez, A., Raposo, M.I.B., Bruguier, O., Oliveira, A.F., 2012. Complex, 3D strain patterns in a synkinematic tonalite batholith from the Araçuaí Neoproterozoic orogen (Eastern Brazil): evidence from combined magnetic and isotopic chronology studies. Journal of Structural Geology 39, 158–179.
Moreira, M.D., 2000. Folha Mucuri. Projeto Leste. CPRM-CODEMIG. http://www.portalgeologia.com.br/mapa/.
Morel, M.L.A., Nebel, O., Nebel-Jacobsen, Y.J., Miller, J.S., Vroon, P.Z., 2008. Hafnium isotope characterization of the GJ-1 zircon reference material by solution and laser-ablation MC–ICPMS. Chemical Geology 255, 231–235.
Nakamura, N., 1974. Determination of REE, Ba, Fe, Mg, Na and K in carbonaceous and ordinary chondrites. Geochimica et Cosmochimica Acta 38, 757–775.
Nalini Jr., H.A., 1997. Caractérisation des suites magmatiques néoprotérozoiques de la region de Conselheiro Pena et Galiléia (Minas Gerais, Brésil). Etude géochimique et structurale des suites Galiléia et Urucum et relations avec les pegmatites à éléments rares associées. Ecole des Mines de Saint Etienne et Ecole des Mines de Paris (Ph.D. Thesis, 237 pp.).
Nalini Jr., H.A., Bilal, E., Correia Neves, J.M., 2000. Syn-collisional peraluminous magmatism in the Rio Doce region: mineralogy, geochemistry and isotopic data of the Urucum suite (eastern Minas Gerais state, Brazil). Revista Brasileira de Geociencias 30, 120–125.
Nalini Jr., H.A., Machado, R., Bilal, E., 2005. Geoquímica e Petrogênese da Suíte Galiléia: Exemplo de Magmatismo Tipo-I Metaluminoso Pré-Colisional Neoproterozóico da Região do Médio Vale do Rio Doce (MG). Revista Brasileira de Geociencias 35, 23–34.
Niu, Y., Zhao, Z., Zhuc, Di-C., Mo, X., 2013. Continental collision zones are primary sites for net continental crust growth — a testable hypothesis. Earth-Science Reviews 127, 96–110.
Noce, C.M., Pedrosa-Soares, A.C., Silva, L.C., Armstrong, R., Danielle Piuzana, D., 2007. Evolution of polycyclic basement complexes in the Araçuaí orogen, based on U–Pb SHRIMP data: implications for Brazil–Africa links in Paleoproterozoic time. Precambrian Research 159, 60–78.
Novo, T.A., Pedrosa-Soares, A.C., Noce, C.M., Alkmim, F.F., Dussin, I., 2010. Rochas charnockíticas do sudeste de Minas Gerais: a raiz granulítica do arco magmático do Orógeno Araçuaí. Revista Brasileira de Geociencias 40, 573–592.
Paes, V.J.C., 2000. Folha Teófilo Otoni. Projeto Leste. CPRM-CODEMIG. http://www.portalgeologia.com.br/mapa/.
Paes, V.J.C., Raposo, F.O., Pinto, C.P., Oliveira, F.A.R., 2010. Projeto Jequitinhonha, Estados de Minas Gerais e Bahia: texto explicativo. Geologia e Recursos Minerais das Folhas Comercinho, Jequitinhonha, Almenara, Itaobim, Joaíma e Rio do Prado, Programa Geologia do Brasil: Belo Horizonte, CPRM (376 pp.).
Pankhurst, R.J., Rapela, C.W., Saavedra, J., Baldo, E.G., Dahlquist, J.A., Pascua, I., Fanning, C.M., 1998. The Famatinian arc in the central Sierras Pampeanas: an early to mid-Ordovician continental arc on the Gondwana margin. In: Pankhurst, R.J., Rapela, C.W. (Eds.), The Proto-Andean Margin of Gondwana. Geological Society, London, Special Publications 142, pp. 343–367.
Patchett, P.J., Tatsumoto, M., 1980. A routine high-precision method for Lu–Hf isotope geochemistry and chronology. Contributions to Mineralogy and Petrology 75, 263–267.
Patiño Douce, A.E., 1999. What do experiments tell us about the relative contributions of crust and mantle to the origin of granitic magmas? In: Castro, A., Fernández, C., Vigneresse, J.L. (Eds.), Understanding Granites: Integrating New and Classical Techniques. Geological Society, London, Special Publications 168, pp. 55–75
Pedrosa-Soares, A.C., Wiedemann-Leonardos, C.M., 2000. Evolution of the Araçuaí belt and its connection to the Ribeira Belt, Eastern Brazil. In: Cordani, U.G., Milani, E.J., Thomaz Filho, A., Campos, D.A. (Eds.), Tectonic Evolution of South America. International Geological Congress, Rio de Janeiro, pp. 265–285.
Pedrosa-Soares, A.C., Noce, C.M., Vidal, P., Monteiro, R.L.B.P., Leonardos, O.H., 1992. Toward a new tectonic model for the Late Proterozoic Araçuaí (SE Brazil)–West Congolian (SW Africa) Belt. Journal of South American Earth Sciences 6, 33–47.
Pedrosa-Soares, A.C., Vidal, P., Leonardos, O.H., Brito Neves, B.B., 1998. Neoproterozoic oceanic remnants in eastern Brazil: further evidence and refutation of an exclusively ensialic evolution for the Araçuaí–West Congo orogen. Geology 26, 519–522.
Pedrosa-Soares, A.C., Noce, C.M., Wiedemann, C.M., Pinto, C.P., 2001. The Araçuaí–West Congo orogen in Brazil: an overview of a confined orogen formed during Gondwanaland assembly. Precambrian Research 110, 307–323.
Pedrosa-Soares, A.C., Alkmim, F.F., Tack, L., Noce, C.M., Babinski, M., Silva, L.C., Martins-Neto, M.A., 2008. Similarities and differences between the Brazilian and African counterparts of the Neoproterozoic Araçuaí–West-Congo orogen. Geological Society, London, Special Publications 294, 153–172.
Pedrosa-Soares, A.C., De Campos, C., Noce, C.M., Silva, L.C., Novo, T., Roncato, J., Medeiros, S., Castañeda, C., Queiroga, G., Dantas, E., Dussin, I., Alkmim, F.F., 2011. Late Neoproterozoic–Cambrian granitic magmatism in the Araçuaí orogen (Brazil), the Eastern Brazilian Pegmatite Province and related mineral resources. Geological Society, London, Special Publications 350, 25–51.
Peixoto, E., Pedrosa-Soares, A.C., Alkmim, F.F., Dussin, I.A., 2015. A suture-related accretionary wedge formed in the Neoproterozoic Araçuaí orogen (SE Brazil) during Western Gondwanaland assembly. Gondwana Research 27 (2), 878–896.
Porada, H., 1989. Pan-African rifting and orogenesis in southern to equatorial Africa and Eastern Brazil. Precambrian Research 44, 103–136.
Queiroga, G.N., Pedrosa-Soares, A.C., Noce, C.M., Alkmim, F.F., Pimentel, M.M., Dantas, E., Martins, M., Castañeda, C., Suita, M.T.F., Prichard, H., 2007. Age of the Ribeirão da Folha ophiolite, Araçuaí orogen: the U–Pb zircon dating of a plagiogranite. Geonomos 15, 61–65.
Rickwood, P.C., 1989. Boundary lines within petrologic diagrams which use oxides of major and minor elements. Lithos 22, 247–263.
Rudnick, R., 1995. Making continental crust. Nature 378, 571–578.
Sampaio, A.R., 2000. Folha Padre Paraíso. Projeto Leste. CPRM-CODEMIG. http://www.portalgeologia.com.br/mapa/.
Silva, L.C., Armstrong, R., Noce, C.M., Carneiro, M., Pimentel, M., Pedrosa-Soares, A.C., Leite, C., Vieira, V.S., Silva, M., Paes, V., Cardoso-Filho, J., 2002. Reavaliação da evolução geológica em terrenos pré-cambrianos brasileiros com base em novos dados U–Pb SHRIMP, parte II: Orógeno Araçuaí, Cinturão Móvel Mineiro e Cráton São Francisco Meridional. Revista Brasileira de Geociencias 32, 513–528.
Silva, L.C., Pedrosa-Soares, A.C., Armstrong, R., Noce, C.M., 2011. Determinando a duração do período colisional do Orógeno Araçuaí com base em geocronologia U–Pb de alta resolução em zircão: uma contribuição para a história da amalgamação do Gondwana Ocidental. Geonomos 19, 180–197.
Sláma, J., Košler, J., Condon, D.J., Crowley, J.L., Gerdes, A., Hanchar, J.M., Horstwood, M.S.A., Morris, G.A., Nasdala, L., Norberg, N., Schaltegger, U., Schoene, B., Tubrett, M.N., Whitehouse, M.J., 2008. Plešovice zircon — a new natural reference material for U–Pb and Hf isotopic microanalysis. Chemical Geology 249, 1–35.
Sun, S.S., McDonough, W.E., 1989. Chemical and isotopic systematics of oceanic basalts: implications for mantle composition and processes. In: Saunder, A.D., Norry, J.M. (Eds.), Magmatism in Ocean Basins. Geological Society, London, Special Publications 42, pp. 313–345.
Tanaka, T., Togashi, S., Kamioca, H., 2000. JNd-1: a neodymium isotopic reference in consistency with La Jolla neodymium. Chemical Geology 168, 279–281.
Tedeschi, M., 2013. Caracterização do arco magmático do Orógeno Araçuaí entre Frei Inocêncio e Itambacuri, MG (Master Thesis), UFMG, Belo Horizonte, Brazil (127 pp.).
Torquato, J.R., Cordani, U.G., 1981. Brazil–Africa geological links. Earth-Science Reviews 17, 155–176.
Tupinambá, M., Heilbron, M., Valeriano, C., Porto Jr., R., de Dios, F.B., Machado, N., Silva, L.G.E., Almeida, J.C.H., 2012. Juvenile contribution of the Neoproterozoic Rio Negro Magmatic Arc (Ribeira Belt, Brazil): implications for Western Gondwana amalgamation. Gondwana Research 21, 422–438.
Vieira, V.S., 2007. Significado do Grupo Rio Doce no Contexto do Orógeno Araçuaí (Ph.D. Thesis), IGC-UFMG, Belo Horizonte, Brasil (117 pp.).
Vielzeuf, D., Holloway, J.R., 1988. Experimental determination of the fluid-absent melting relations in the pelitic system. Consequences for crustal differentiation. Contributions to Mineralogy and Petrology 98, 257–276.
Villaros, A., Buick, I.S., Stevens, G., 2012. Isotopic variations in S—type granites: an inheritance from a heterogeneous source? Contrib. Mineral. Petrol. 163 (2), 243–257.
Villaseca, C., Barbero, L., Herreros, V., 1998. A re-examination of the typology of peraluminous granite types in intracontinental orogenic belts. Transactions of the Royal Society of Edinburgh: Earth Sciences 89, 113–119.
Wu, F.Y., Yang, Y.H., Xie, L.W., Yang, J.H., Xu, P., 2006. Hf isotopic compositions of the standard zircons and baddeleyites used in U–Pb geochronology. Chemical Geology 234, 105–126.